Report No: 9102-01 OF
Contract No: C89-19

Final Report

to

Center for Transportation Studies
110 Civil and Mineral Engineering
University of Minnesota
500 Pillsbury Drive, S.E.
Minneapolis, MN 55455

# CORROSION INVESTIGATION OF REINFORCING BARS IN PAVEMENTS AND BRIDGE DECKS

## PART II. CHLORIDE PENETRATION/REBAR CORROSION MECHANISMS

by

J.W. Jang and I. Iwasaki

February 25, 1991

MINERAL RESOURCES RESEARCH CENTER
DEPARTMENT OF CIVIL AND MINERAL ENGINEERING

UNIVERSITY OF MINNESOTA

Final Report

to

Center for Transportation Studies
110 Civil and Mineral Engineering
University of Minnesota
500 Pillsbury Drive, S.E.
Minneapolis, MN 55455

# CORROSION INVESTIGATION OF REINFORCING BARS IN PAVEMENTS AND BRIDGE DECKS

## PART II. CHLORIDE PENETRATION/REBAR CORROSION MECHANISMS

by

J.W. Jang and I. Iwasaki

February 19, 1991

Mineral Resources Research Center
Department of Civil and Mineral Engineering
University of Minnesota
56 East River Road
Minneapolis, MN 55455

## SUMMARY

The main factors that influence the initiation and propagation of rebar corrosion in concrete are concrete properties, aggressive corrosive elements from the environment and concrete, and defects of the reinforcing material. The presence of chloride ion appears to be the dominant cause for rebar corrosion in concrete. Rebar corrosion is complex and the basic mechanisms of individual factors are not well understood because of the complex nature of physical and electrochemical factors and because of their interdependence.

A visualization technique was developed for use in our laboratory for the determination of chloride ion distribution and concentration near the reinforcements in concrete. A galvanic current measurement technique was developed for estimating the corrosion rates of rebars in simulated concrete solutions and for investigating the effects of relevant parameters that may be responsible for macro-cell corrosion on rebars as a function of chloride ion concentration. The corrosion mechanism of rebars was explored by using the galvanic current measurement method as well as by using optical and scanning electron microscopy.

The compounds that combine the properties of a corrosion inhibitor and a surfactant were explored for retardation of rebar corrosion. Organic compounds slowed the corrosion of rebars acting as an adsorption-type inhibitor. Organic compounds developed hydrophobic surfaces on concrete. Such an observation implies that salt solution may be prevented from penetrating the microcracks in concrete.



*The financial support of oil overcharge funds distributed through the Minnesota Department of Administration is acknowledged, but the authors assume complete responsibility for the contents herein.*

## CONTENTS


Page

LIST OF FIGURES ..... ii

INTRODUCTION ..... 1

EXPERIMENTAL ..... 4
1. Field Samples ..... 4
2. Visualization Technique ..... 4
3. Electrochemical Measurements ..... 6
4. Evaluation of Salt Additives ..... 9

RESULTS ..... 9
1. Optical and Scanning Electron Microscope Observation of Corroded Rebar ..... 9
2. Chloride Concentration and Distribution in Concrete ..... 12
3. Galvanic Current Measurements ..... 14
4. Salt Additives ..... 18

DISCUSSION ..... 22
1. Chloride Concentration and Distribution in Concrete ..... 23
2. Electrochemical Measurement Technique for Rebar Corrosion ..... 24
3. Mechanisms of Rebar Corrosion ..... 25
4. Retardation of Rebar Corrosion ..... 27

CONCLUSIONS ..... 29

REFERENCES ..... 30

Appendix I. "Visualization of Chloride Distribution in Concrete," J.W. Jang and I. Iwasaki, Transportation Research Board, 70th Annual Meeting, January 13-17, 1991, Washington, D.C., preprint No. 910156 and also in print at Transportation Research Board Journal.

Appendix II. "Rebar Corrosion Under Simulated Concrete Conditions Using Galvanic Current Measurements," J.W. Jang and I. Iwasaki, Transportation Research Board, 70th Annual Meeting, January 13-17, 1991, Washington, D.C., preprint No. 910155.

## FIGURE LISTS


Page

Figure 1. Visualization results for chloride ion distribution and concentration in concrete; (a) concrete sample with rebar, (b) color map, and (c) calibration strips. . . . . 5

Figure 2. Schematic representation of experimental set-ups for galvanic current measurements of reinforcements in (a) a simulated concrete environment, and (b) a concrete block. . . . . 7

Figure 3. Corroded reinforcements with and without concrete blocks collected from the field: (a) and (b) concrete cracks around corroded reinforcements, (c) severe corrosion near grid-intersections, (d) and (e) localized corrosion near material defects (inclusions) and welded areas, and (f) reinforcement volume changes by corrosion. . . . . 10

Figure 4. Surfaces of corroded reinforcement by scanning electron microscopy: (a) sharp cracks on oxide layer, (b) irregular cracks in reinforcement metal matrix, (c) and (d) corrosion initiation and propagation along grain boundaries of reinforcement material, (e) a space between oxide layer and metal matrix, and (f) crack propagation on oxide layer by fatigue stresses. . . . . 11

Figure 5. Cross section of corroded reinforcement by optical microscopy: (a) and (b) severe corrosion beneath the surface, (c) preferential corrosion on pearlite structure, and (d) corrosion propagation along the grain boundaries of reinforcement material. . . . . 13

Figure 6. Galvanic current and combination potential as a function of time at different chloride concentrations. . . . . 15

Figure 7. Corroded areas (indicated by a) on reinforcement surface showing the effect of chloride ion concentration. . . . . 16

Figure 8. (a) Comparison of galvanic currents obtained by the concrete chip method (Figure 2(a)) and the concrete block method (Figure 2(b)), and (b) chloride movement by diffusion as a function of distance from concrete surface to rebar (Equation (4)). . . . . 17

Figure 9. Effect of deformation and welding on galvanic corrosion currents of reinforcement. . . . . 19

Page

Figure 10. Salt additives as an inhibitor; (a) optimum dosage, (b) effect of inhibitors and (c) inhibitor efficiency . . . . . 20

Figure 11. Effect of additives on wettability. Air bubbles are attached to concrete pieces under additive conditions . . . . . 21

Figure 12. Schematic diagram for a possible method of corrosion retardation by chemical additives to salt . . . . . 28

# INTRODUCTION

The main factors that influence the initiation and propagation of rebar corrosion in concrete are concrete properties, aggressive corrosive elements from the environment and concrete, and defects of the reinforcing material. The presence of chloride ion appears to be the dominant cause for rebar corrosion in concrete.

The electrochemical corrosion in concrete may occur because of the non-uniformities of the reinforcing steel (different steels, welds, active sites on the steel surface) (1), or of chemical or physical environments in the surrounding concrete (2). These non-uniformities under certain specific conditions can produce significant electric potential differences and resultant corrosion. Macro-cell corrosion in rebars due to the difference in chloride ion concentration as well as the structural and compositional defects of rebars in concrete could accelerate the localized corrosion.

Rebar corrosion is complex and the basic mechanisms of individual factors are not well understood because of the complex nature of physical and electrochemical factors and because of their interdependence. Many research efforts (3,4) have been made in the last two decades which contributed to the understanding of rebar corrosion, to the development of monitoring methods and to the protection methods of rebars. However, many contradictory experimental results and views have been reported on the deterioration behavior of reinforced concrete structures.

Corrosion rates of rebars can be determined by measuring weight losses only after the concrete structure is destroyed. Since the corrosion of rebars is electrochemical in nature, many approaches (5,6) have been tried to develop electrochemical methods for testing. However, various fundamental and experimental factors contribute to the

inaccuracies in these results. The linear polarization and polarization resistance techniques of monitoring corrosion rates in concrete has uncertain factors such as the location of counter and reference electrodes and the material of the counter electrode (5). In addition, these techniques are not applicable for a continuous monitoring of corroding rebars in situ over extended periods of time, while a galvanic current measurement technique is capable of such measurements. The method has been used successfully in an investigation on the corrosion mechanism of grinding media under dynamic conditions in our laboratory for the past 15 years (7-9).

Localized corrosion of reinforcements in concrete is caused by the impurities of the reinforcement material, deformation of the reinforcement surfaces, concentration difference of chloride ion near the reinforcement, and the complex interactions of the above factors (10,11). Deformed and/or defect surfaces of reinforcements could be the corrosion initiation sites even under very low chloride ion concentrations because of their thermodynamic instabilities, while no corrosion may be found on the deformation-free and/or defect-free surfaces under relatively high chloride ion concentrations. Galvanic interactions between corroding and non-corroding areas accelerate the localized corrosion at the surfaces of reinforcements.

Similarly, the concentration differences of chloride ion near reinforcements create galvanic cells between the high and low or no chloride concentration surfaces of the reinforcements (11). High chloride concentration areas become the anode, and low or no chloride concentration areas the cathode. Corrosion rates increase as the chloride concentration difference increases.

Chloride contents of concrete are usually measured by dry drilling and chemical analysis of the drilled samples. However, the conventional method does not provide any information on chloride distribution near the reinforcement in concrete, particularly along hair-line cracks. Such an information would be essential in understanding the localized corrosion mechanisms and kinetics.

The use of de-icing salts accelerates rebar corrosion in bridge decks and parking ramps as mentioned previously. The compounds that combine the properties of a corrosion inhibitor and a surfactant that imparts water-repellent coating on concrete would prevent the penetration of salt solutions through pores and cracks in concrete, and even when the salt solution reaches the rebar, the surfactants adsorb on the rebar surfaces and act as corrosion inhibitors.

The purpose of the present investigation was to develop,

(i) a visualization technique in use in our laboratory for the determination of chloride ion distribution and concentration near the reinforcements in concrete, and

(ii) a galvanic current measurement technique for estimating the corrosion rates of rebars in simulated concrete environments and for investigating the effects of relevant parameters that may be responsible for macro-cell corrosion on rebars as a function of chloride ion concentration.

The corrosion mechanisms of rebars were explored by using the galvanic current measurement method as well as by using optical and scanning electron microscopy. The compounds that combine the properties of a corrosion inhibitor and a surfactant were explored for retardation of rebar corrosion.

## EXPERIMENTAL

1. Field Samples

Rebar samples with and without concrete blocks were collected from the I-94 bridge deck in front of the State Capital, St. Paul and the I-94 Lowry Hill Tunnel pavement in Minneapolis, Minnesota. The diameter of the rebars was ½ inch, and the chloride content in a concrete sample analyzed 1100 ppm. The rebars were examined for corrosion behavior and corrosion initiation sites through observation of the surfaces under a JEOL 840 II scanning electron microscope and the cross section by an Olympus microscope model PM-10AD.

The rebar samples for scanning electron microscopy were cleaned by dipping in 10% hydrochloric acid for 5 seconds and by rinsing with distilled water. The rinsed samples were dried with 99% isopropyl alcohol and blowing air over them.

The cross-cut rebars were cold-mounted in epoxy and polished using conventional metallographic polishing techniques and etched with 2% Nital solution.

2. Visualization Technique

Concrete blocks containing reinforcements were collected in the field, cut and ground to expose flat smooth surfaces. The concrete surfaces were finished with 320 grit silicon carbide abrasive papers. A crack was intentionally made from one edge of the concrete block to the reinforcement as shown in Figure 1(a). A solution of 10% $CaCl_2$ was applied repeatedly to the crack in order to simulate the chloride penetration through the crack.

The indicator solutions used for detection and determination of chloride ion on the surface of the concrete block were 0.025% mercuric nitrate in 0.008M nitric acid, and 0.25% diphenylcarbazone in methanol. A filter paper was wetted by the mercuric nitrate solution

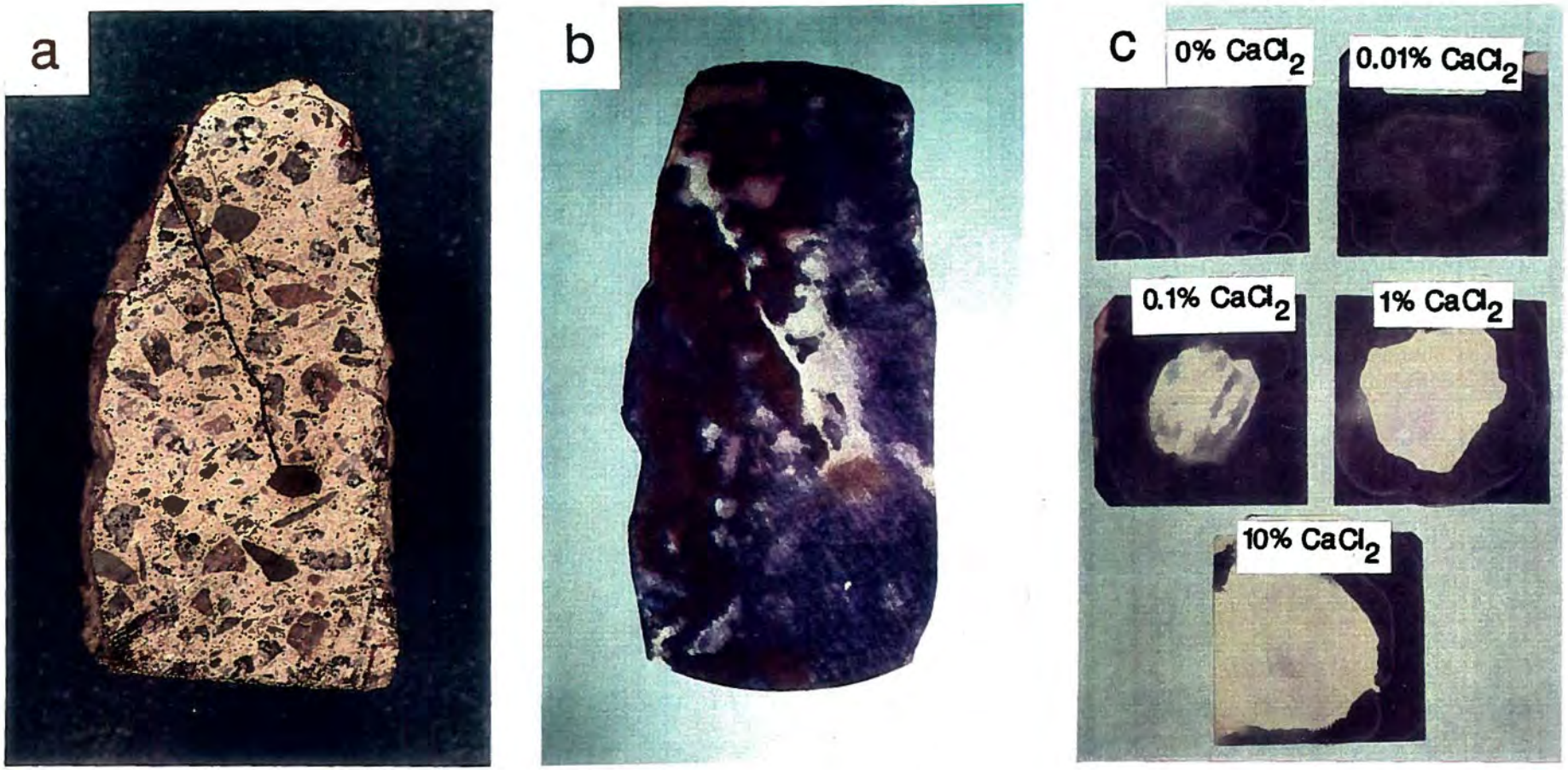


Figure 1. Visualization results for chloride ion distribution and concentration in concrete; (a) concrete sample with rebar, (b) color map, and (c) calibration strips.

uniformly. The filter paper was placed over the flat smooth concrete block, pressed firmly with a roller and left standing for a few minutes. Then the filter paper was peeled off and the diphenylcarbazone solution was sprayed over it, and air dried. For the purpose of calibration, 0, 0.01, 0.1, 1 and 10% $CaCl_2$ solutions were also applied to filter papers, and the color was developed as before.

3. Electrochemical Measurements

A galvanic current measurement method was chosen for investigating the effect of chloride ion concentration on rebar corrosion in concrete. A laboratory galvanic cell was made by dipping two rebars in chloride-containing and chloride-free solutions and short-circuiting them, as shown in Figure 2(a). The test solutions were prepared by saturating 500 ml deionized water with 25g of concrete chips of approximately 1/8" in size in a series of 600 ml beakers and adding 0, 0.1, 1 and 10% calcium chloride in one set of beakers and none in the other set in order to simulate the chemistry of concrete environments. The pH of the concrete chip saturated solution was 12. 5. To compensate for the evaporation loss, the solution levels were maintained constant by frequent addition of distilled water. The chemical composition of the rebars was determined by spectrographic analysis as follows:

| C | Mn | P | S | Si | Sn | Cu | Ni | Cr | Mo |
|---|---|---|---|---|---|---|---|---|---|
| 0.35 | 0.72 | 0.021 | 0.053 | 0.03 | 0.009 | 0.04 | 0.04 | 0.05 | 0.10 |

The ½" rebar samples were made into electrodes by attaching an electrical wire to ¼" high steel pieces with a silver conductive epoxy and by mounting in epoxy. After the epoxy

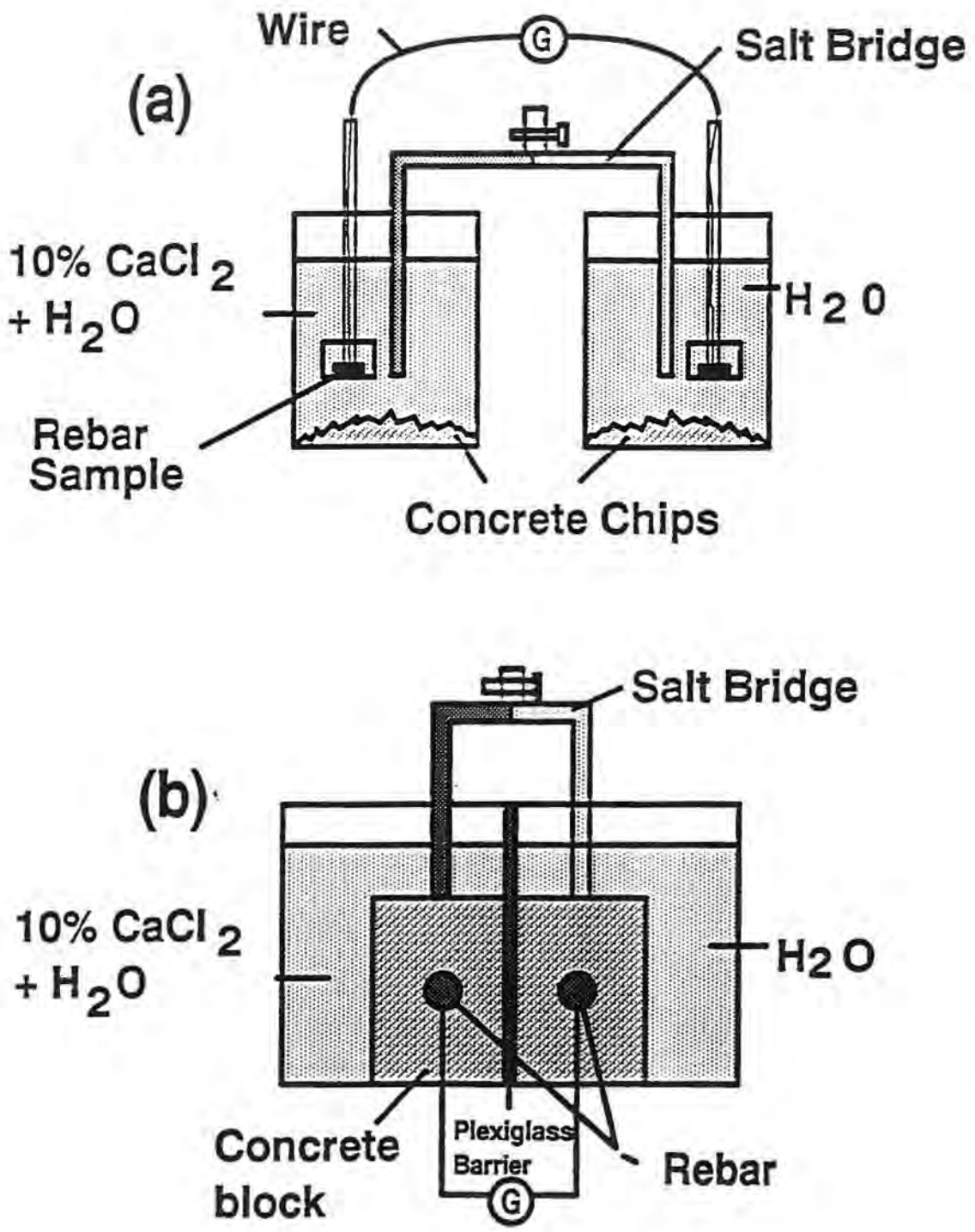


Figure 2. Schematic representation of experimental set-us for galvanic current measurements of reinforcements in (a) a simulated concrete environment, and (b) a concrete block.

hardened, the bottom surfaces of the mounted rebars were ground and polished. A Lucite tube of ¼" I.D. was attached to the other flat surface by using 5-minute epoxy.

To test the relevance of the foregoing beaker-scale method, galvanic current measurements were made between two rebars imbedded in a concrete block obtained from the field. The concrete block had an overall dimension of 2.0 x 5.0 x 2.5 inch, and the ½ inch diameter rebars were imbedded 2 inches apart. The concrete was analyzed to contain approximately 1100 ppm $Cl^-$. The concrete block was divided into two sides with a barrier as shown in Figure 2(b). One side was filled with 10% $CaCl_2$ solution and the other filled with deionized water. The rebars were short-circuited and the galvanic currents between the two were monitored as a function of time.

The effects of welded and bent rebars on galvanic corrosion in concrete was investigated by using a galvanic cell setup mentioned earlier (Figure 2(a)) by dipping and short-circuiting normal and welded or bent rebars in 10% $CaCl_2$ solution saturated with concrete chips as described earlier in an attempt to simulate the concrete environment. Localized strain of a bent rebar was induced by a three point loading. The bend angle of the ½ inch diameter rebar was approximately 30°. A welded sample was prepared by a shield-metal arc welding method. The weld was made on a ½" diameter rebar using Lincoln E7024 flux electrode and d.c. straight polarity with a Miller model 330A/BP welding machine. The welded rebar sample was ground to a smooth surface after the slag was removed.

All the measurements were made with an EG & G model 350 A corrosion measurement console. A saturated calomel electrode (SCE) was used as the reference electrode via a salt bridge containing a saturated solution of ammonium nitrate.

4. Evaluation of Salt Additives

As a corrosion prevention or retardation method, three chemical additives were investigated by using the galvanic current measurement method as shown in Figure 2(a). A rebar sample dipped in a concrete chip saturated solution containing 10% calcium chloride was short-circuited with another rebar sample in a concrete chip saturated solution free of the salt. Different amounts of chemical additives were added to the concrete chip saturated solution containing 10% calcium chloride, and the galvanic currents were monitored by the EG&G model 350A corrosion measurement console.

To investigate the additives for their surfactant properties, the wettability of concrete surface was determined by measuring the contact angle of an air bubble on concrete pieces.

## RESULTS

1. Optical and Scanning Electron Microscope Observations of Corroded Rebars.

Figure 3(a) and (b) show typical field samples of corroded rebars in concrete with yellow stains of corrosion products and concrete cracks by the corroded rebars. Severe localized corrosion of the rebars was found near grid-intersections (Figure 3(c)), material defects (inclusions) (Figure 3(d)) and welded areas (Figure 3(e)). Figure 3(f) shows that the rebar lost more than a half of the volume from the original rebar by corrosion.

The surfaces of corroded rebars were examined under a scanning electron microscope. Figure 4 shows numerous sharp cracks on the rust layer (a) and irregular cracks on the rebar metal matrix (b). The photomicrographs (Figure 4(c) and (d)) of corroded rebar surfaces indicate that the corrosion of rebars was initiated and propagated along the grain boundaries of the rebar material microstructure, especially carbide

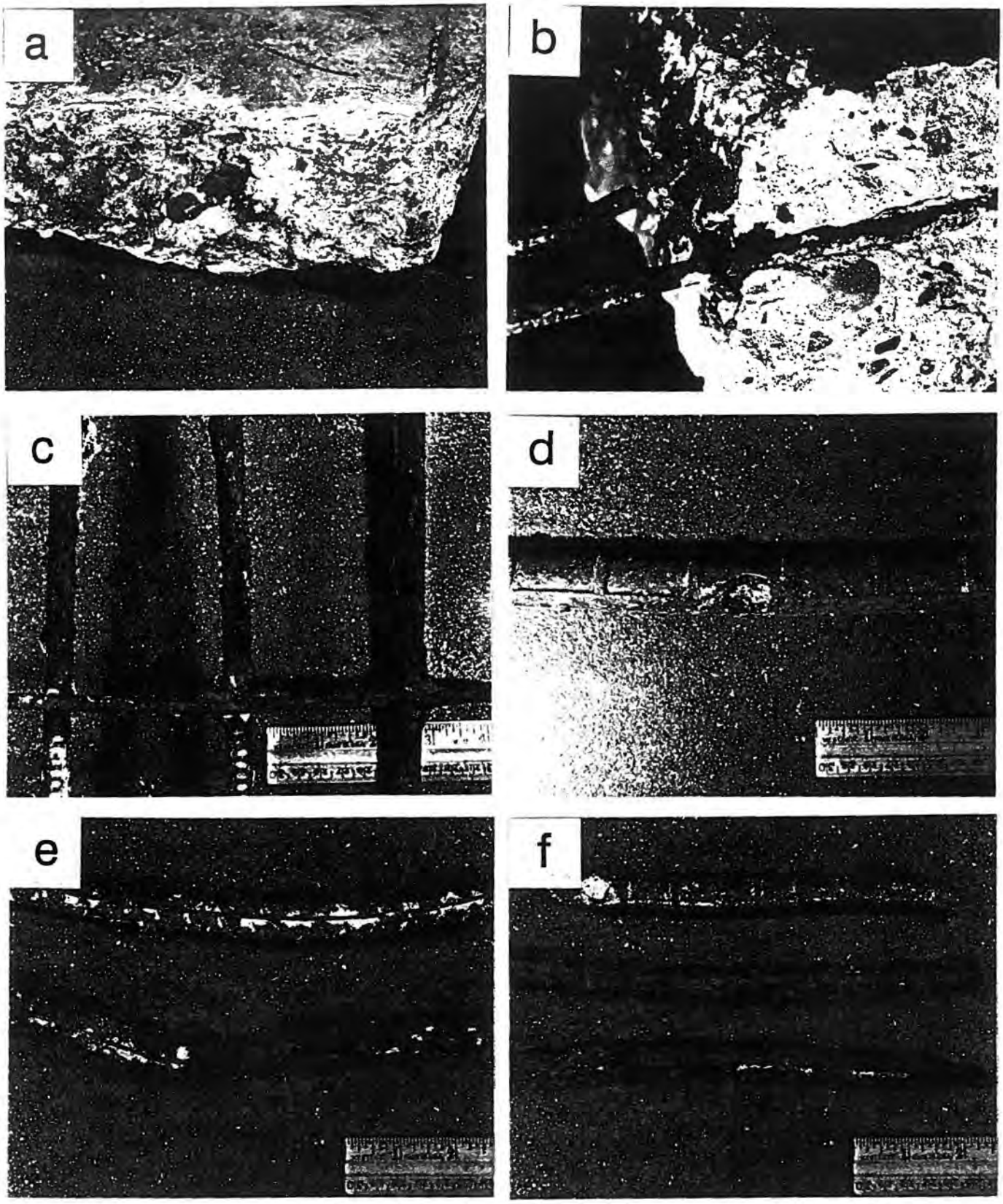


Figure 3. Corroded reinforcements with and without concrete blocks collected from the field: (a) and (b) concrete cracks around corroded reinforcements, (c) severe corrosion near grid-intersections, (d) and (e) localized corrosion near material defects (inclusions) and welded areas, and (f) reinforcement volume changes by corrosion.

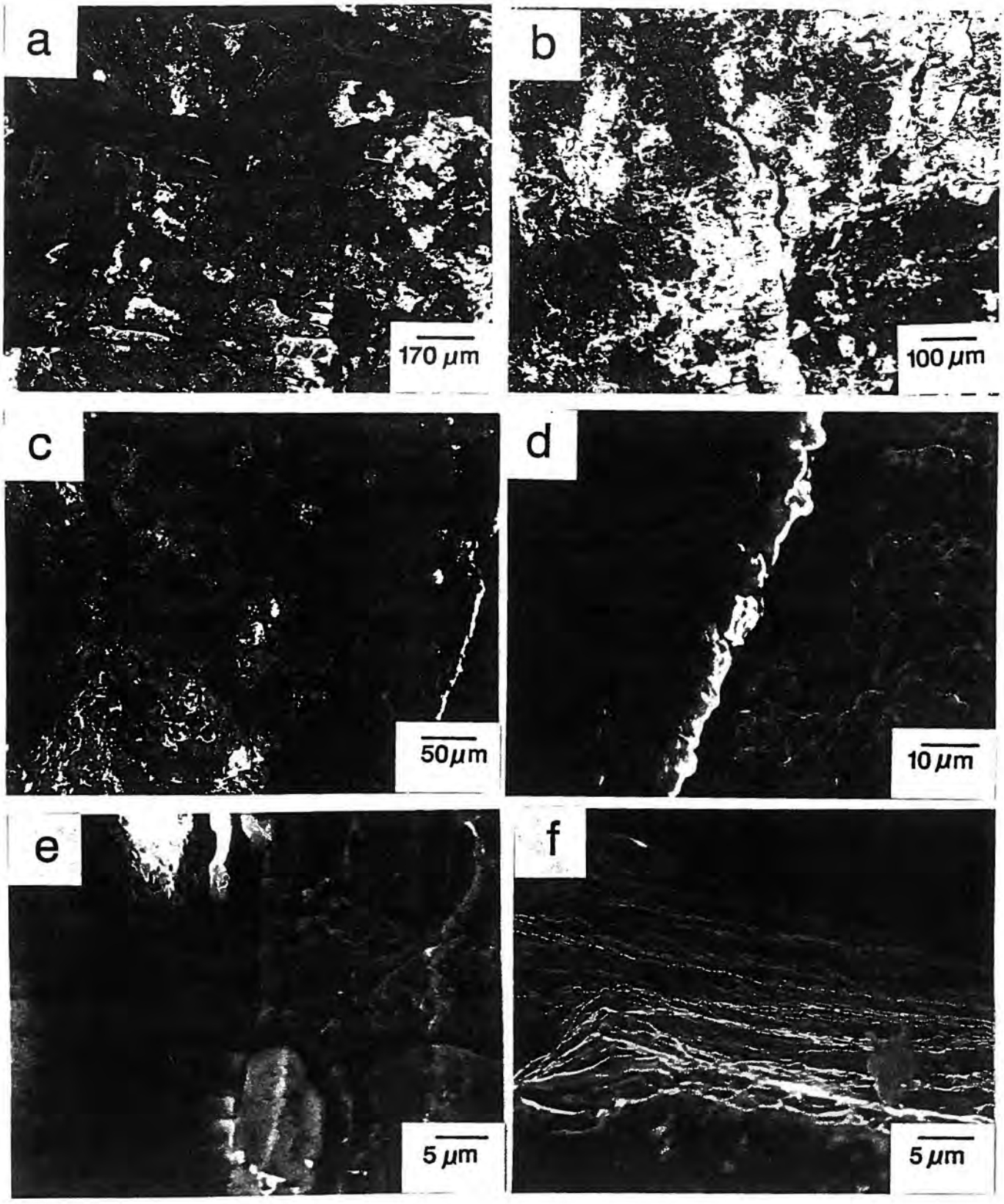


Figure 4. Surfaces of corroded reinforcement by scanning electron microscopy: (a) sharp cracks on oxide layer, (b) irregular cracks in reinforcement metal matrix, (c) and (d) corrosion initiation and propagation along grain boundaries of reinforcement material, (e) a space between oxide layer and metal matrix, and (f) crack propagation on oxide layer by fatigue stresses.

(cementite). Also, there was a space between the rust layer and the metal matrix (Figure 4(e)), which was large enough for chloride ion to spread throughout the whole rebar. The parallel and continuous lines (striations) in Figure 4(f) suggest that the cracks on the oxide layer propagated by fatigue stresses due to vibration (12).

The corroded rebars were cut, and the cross sections examined under an optical microscope. Figures 5(a) and (b) show that even though the surfaces of corroded rebars appeared smooth, severe corrosion was taking place underneath. Conventional rebar materials are mild steel, which consists of ferrite (white in Figure 5) and pearlite (dark) structures. Figure 5(c) shows that the pearlite structure was attacked preferentially, and that the ferrite structure survived longer than the pearlite structure under corrosive conditions in concrete. Figure 5(d) was obtained by using a polarized filter, which shows that the corrosion of the rebar propagated along the grain boundaries of the rebar material microstructures.

2. Chloride Concentration and Distribution in Concrete

The color map of Figure 1(b) shows the chloride ion distribution and concentration in the concrete. The light area indicates where chloride ion is present, and the different shades of purple represent chloride ion concentrations which may be estimated from the calibration strips shown in Figure 1(c). The technique is simple and rapid for the determination of chloride ion concentration and its distribution in concrete.

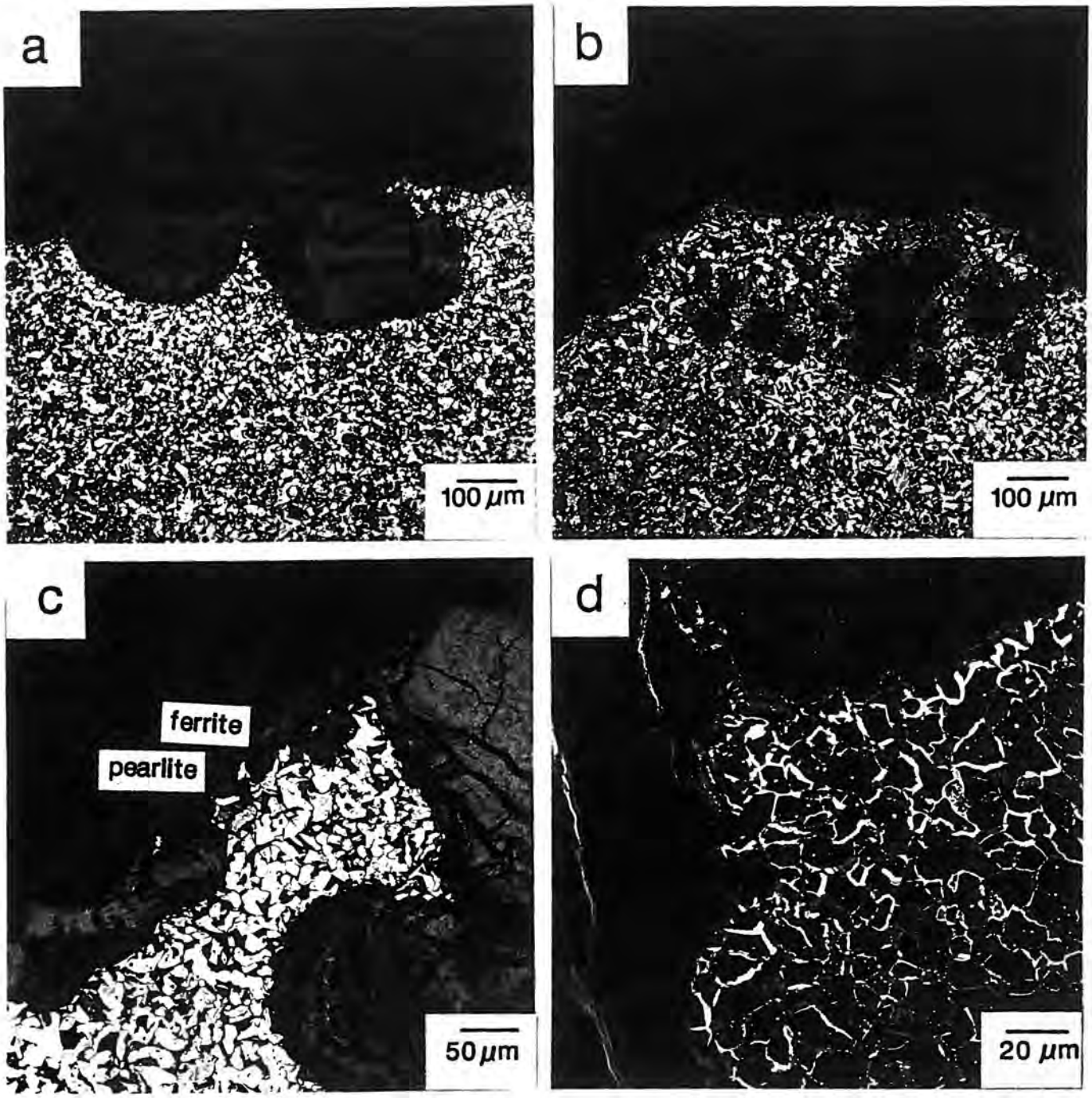


Figure 5. Cross section of corroded reinforcement by optical microscopy: (a) and (b) severe corrosion beneath the surface, (c) preferential corrosion on pearlite structure, and (d) corrosion propagation along the grain boundaries of reinforcement material.

3. Galvanic Current Measurements

Combination potentials and galvanic currents of rebars were obtained at different chloride ion concentrations as a function of time by using the galvanic current measurement method shown in Figure 2(a), and the results are presented in Figure 6. The galvanic currents increased with increasing chloride ion concentration until visible yellow corrosion products appeared on the rebar sample surfaces as indicated by arrows in Figure 6(a). After the corrosion products appeared, the galvanic currents increased dramatically in 0, 0.1 and 1% $CaCl_2$ solutions. In 10% $CaCl_2$ solution, the galvanic current increased and then decreased when the corrosion products appeared. The combination potentials were most active in 10% $CaCl_2$, followed by 1, 0, and 0.1% $CaCl_2$. The combination potentials are seen to cross over randomly after 100 days as shown in Figure 6(b).

The surfaces of rebar samples were examined for their corrosion behaviors after completing the galvanic current measurements. The results are shown in Figure 7. The left-side photos show the surfaces of rebar samples recovered from the solutions containing chloride ion, while the right-side photos are from the chloride-free solutions. The yellow corrosion products on the rebar samples can be seen only in the left-side photos. The rebar samples in the chloride solutions acted as anodes and those in the chloride-free solutions acted as cathodes. It is apparent that those samples which acted as cathodes (right-side photos) are all free of rust. The figure also shows that the corroded areas on the surfaces of rebar samples increased with increasing chloride ion concentration in the solution, and hence with increasing galvanic currents.

The galvanic currents of rebars imbedded in a concrete block (Figure 2(b)) were measured and the results are shown in Figure 8. The galvanic currents decreased initially,

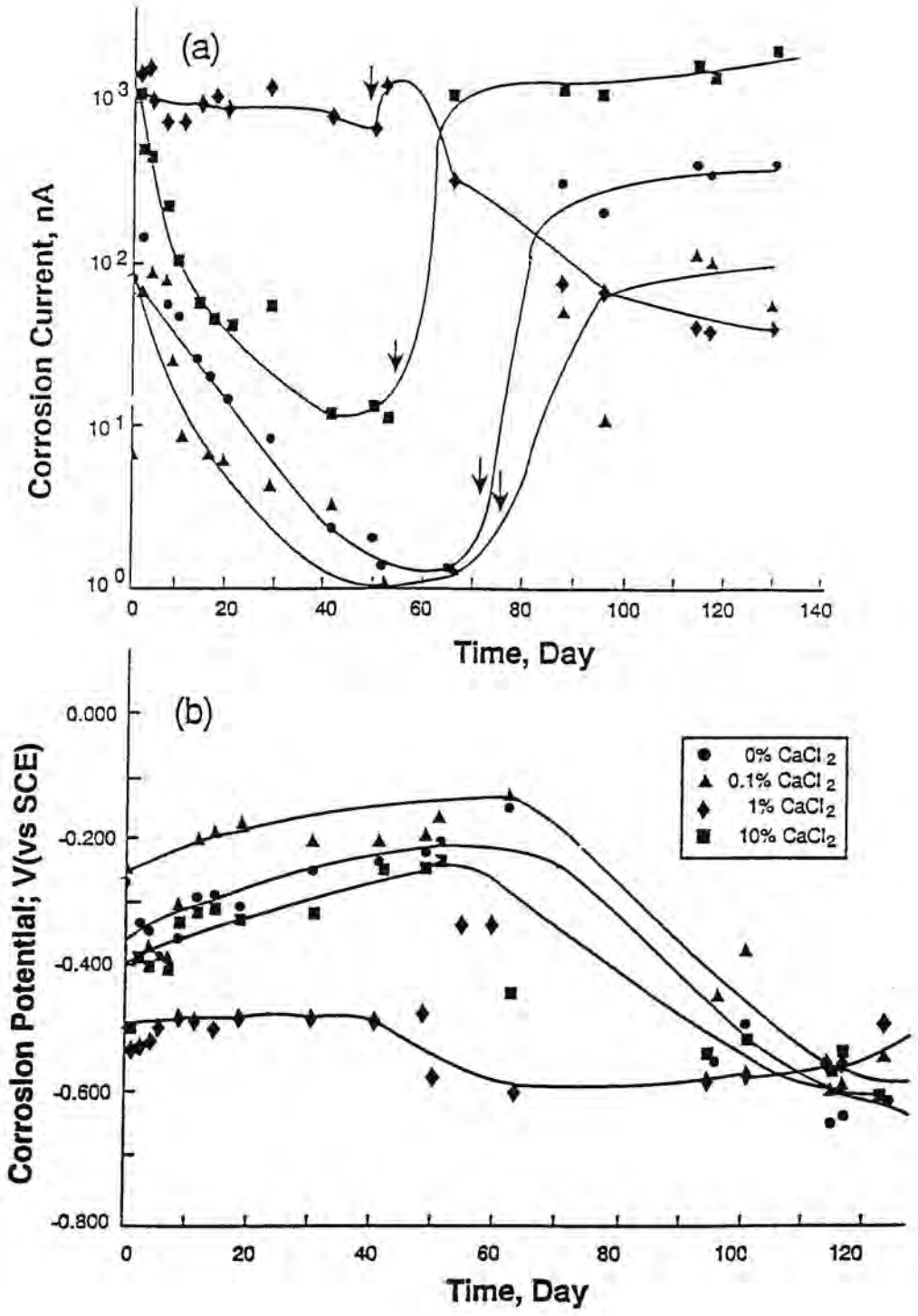


Figure 6. Galvanic current and combination potential as a function of time at different chloride concentrations.

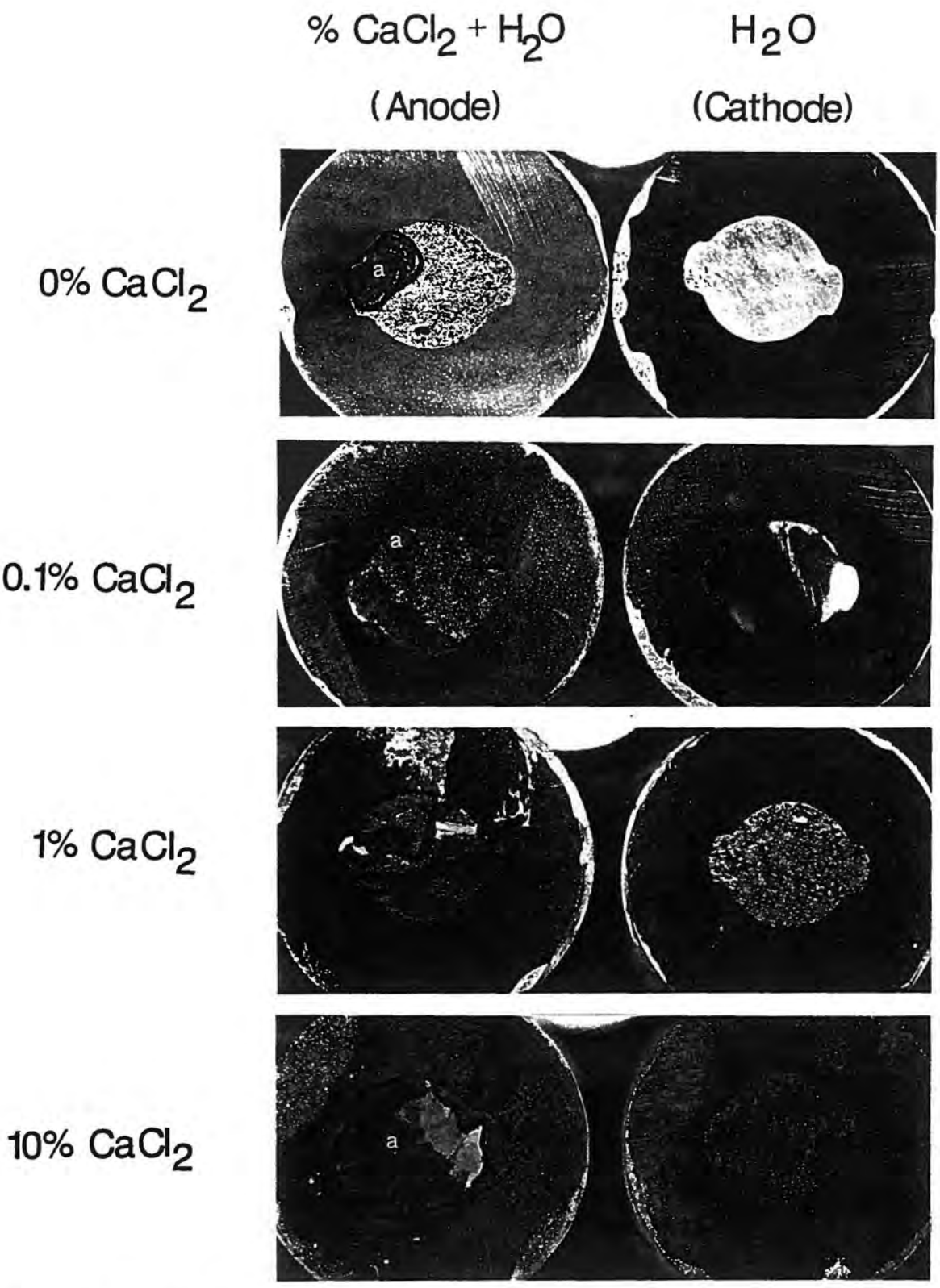


Figure 7. Corroded areas (indicated by **a**) on reinforcement surface showing the effect of chloride ion concentration.

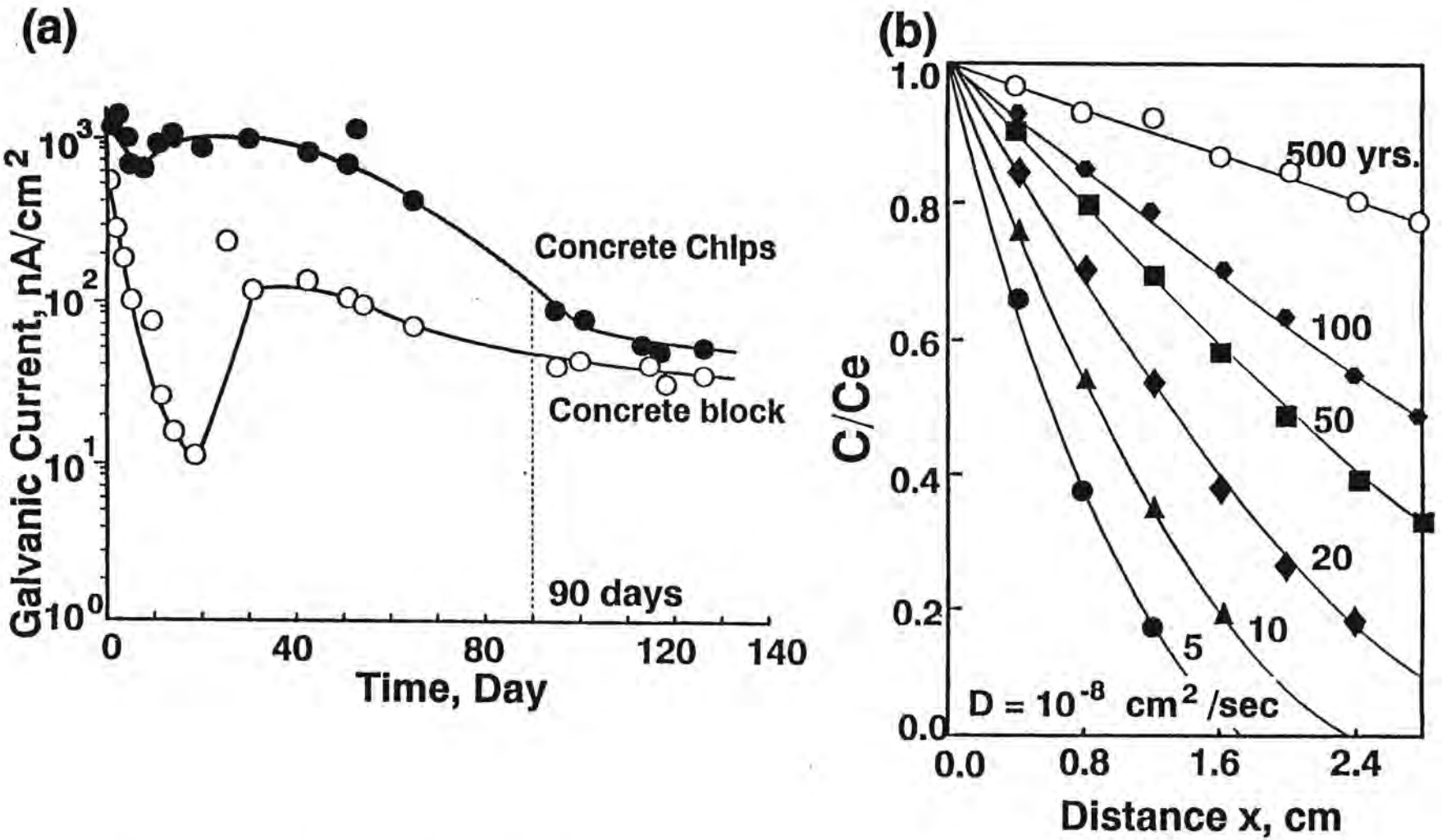


Figure 8. (a) Comparison of galvanic currents obtained by the concrete chip method (Figure 1(a)) and the concrete block method (Figure 1(b)), and (b) chloride movement by diffusion as a function of distance from concrete surface to rebar (Equation (2)).

and then increased. After 50 days, the galvanic currents decreased, and eventually approached the galvanic currents obtained in the simulated concrete environments (Figure 2(a)).

The galvanic currents of the normal, bent and welded rebars were obtained by using the galvanic cell (Figure 2(a)) as a function of time and the results are plotted in Figure 9. The galvanic currents of bent and welded rebars decreased with time, and those of normal rebar decreased initially, then increased somewhat and remained constant thereafter. Note that the galvanic currents of welded and bent rebars were two orders of magnitude higher than those of normal rebar.

4. Salt Additives

The optimum dosage of salt additives was determined by the galvanic current measurements. The amount of additives to the concrete chip saturated solution containing 10% $CaCl_2$ was varied from 0.001, 0.01, 0.1 to 1%. Figure 10(a) shows that 0.01% of the additives provided the best performance as an inhibitor. Figure 10(b) illustrates the effect of 0.01% additives on the galvanic currents of the rebars in the concrete chip saturated solution containing 10% $CaCl_2$. The decrease in the galvanic currents (Figure 10(b)) provide the inhibitor efficiency ranged from 15 to 20% as shown in Figure 10(c).

Another significant observation of the additive was that air bubbles remained attached to the concrete pieces (Figure 11) indicating that the concrete surface was made hydrophobic. The contact angle was zero when there was no additive, while the concrete surface gave finite contact angles when the additives were used. Figure 11 suggests that the additive could act as a surfactant in concrete cracks.

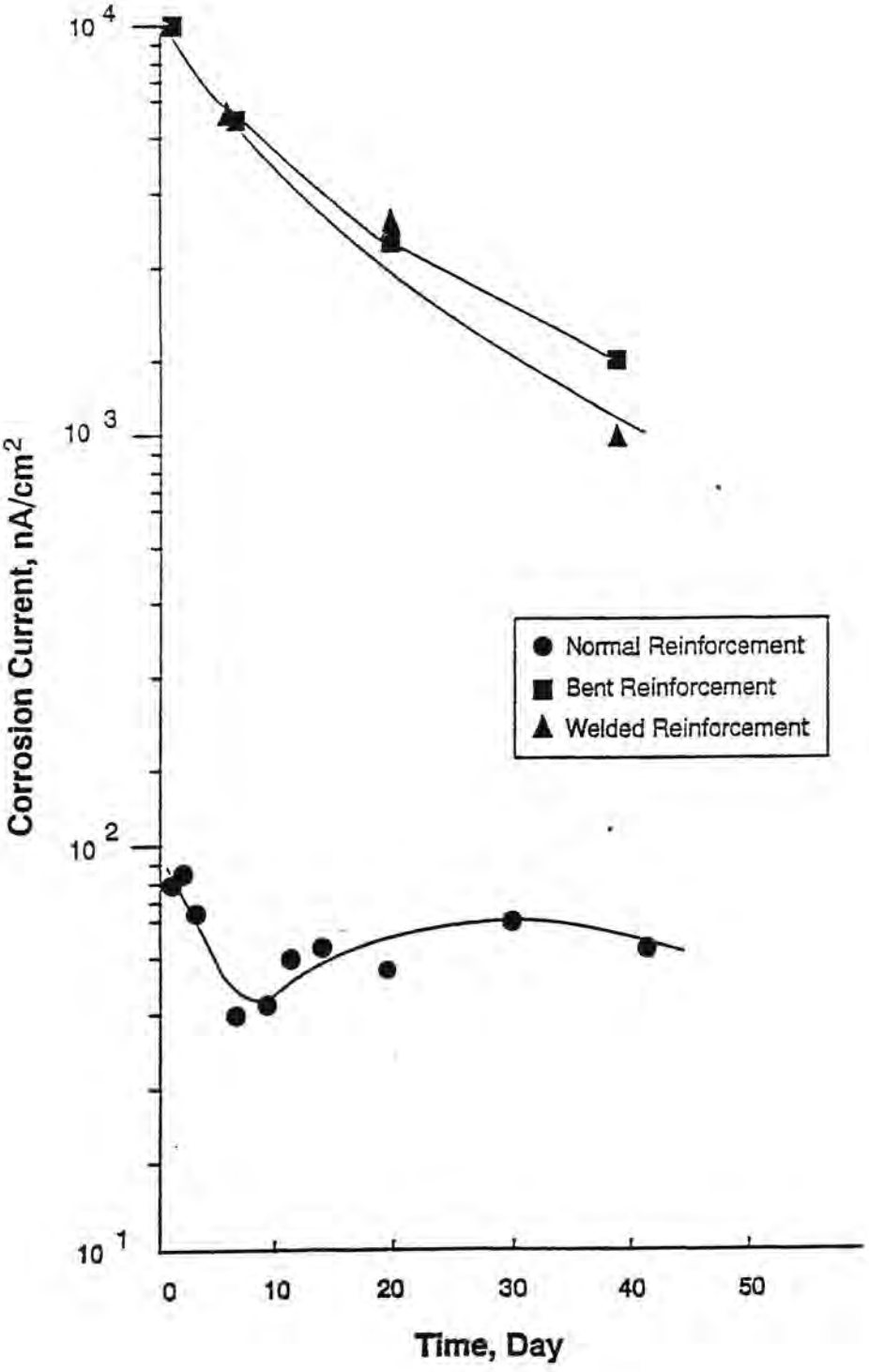


Figure 9. Effect of deformation and welding on galvanic corrosion currents of reinforcement.

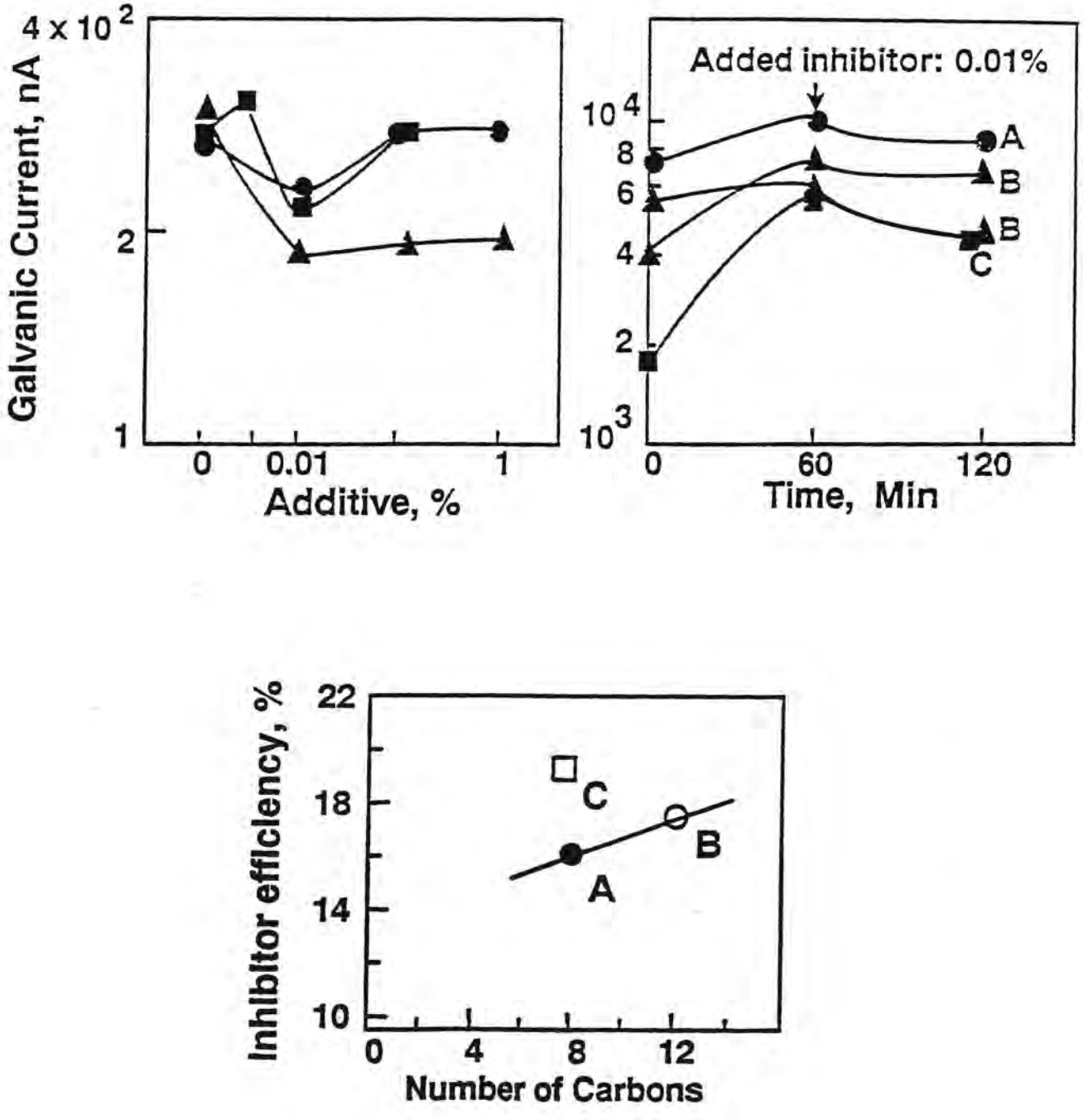


Figure 10. Salt additives as an inhibitor; (a) optimum dosage, (b) effect of inhibitors and (c) inhibitor efficiency.

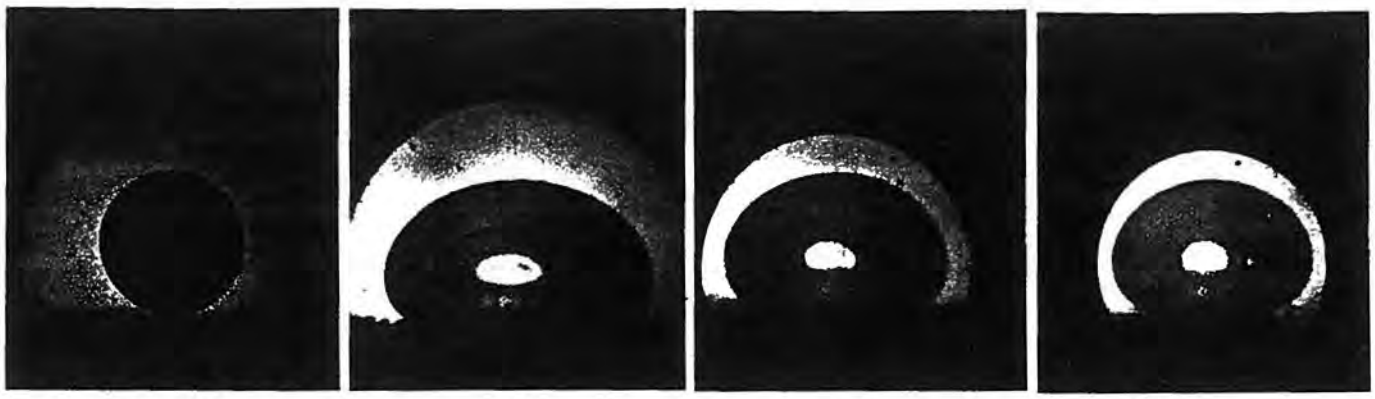


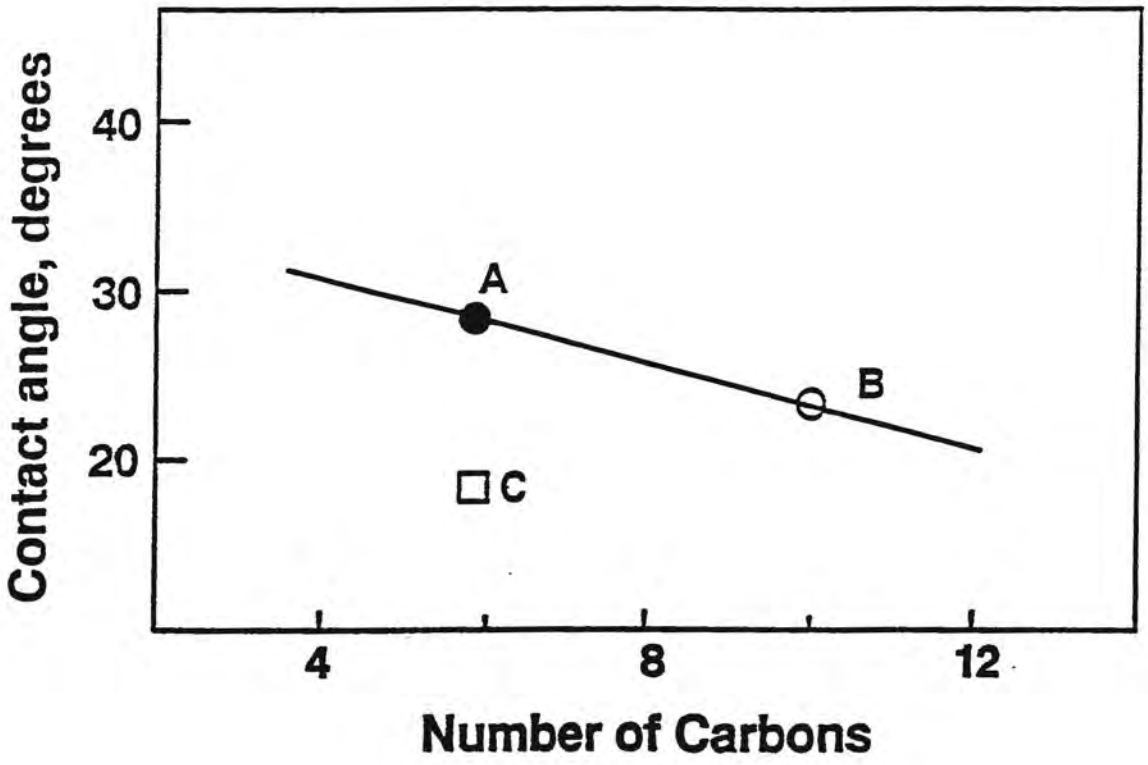


Figure 11. Effect of additives on wettability. Air bubbles are attached to concrete pieces under additive conditions.

## DISCUSSION

Conventional rebar materials are mild steel. The usual impurities have no significant effect on the corrosion rate in atmosphere, neutral water, or soil, but have a marked effect in the case of acid and chloride attacks (13). The presence of sulfur in the form of inclusions markedly increases the rate of attack. Small additions of copper, chromium, and/or nickel (14), and the reduction of sulfur (inclusions) decrease the corrosion rates of rebars significantly in chloride environments.

Galvanic cells between dissimilar constituents (e.g., ferrite and pearlite) of a mild steel structure, and between constituents and inclusions along the grain boundaries could accelerate the rebar corrosion as shown in Figures 4 and 5. Differences in potentials between the dissimilar constituents of the structure cause electron flow between them when they are electrically coupled (9). Direction of the current flow (galvanic behavior) depends on which constituent is more active. Thus, the more active constituent becomes the anode, and the more noble constituent becomes the cathode in the couple. The driving force for galvanic corrosion is the difference in potential between the constituents. Figure 5(c) suggests that the pearlite was the anode and the ferrite was the cathode.

The use of deicing salts in winter could develop a strong galvanic corrosion cell between the rebars in chloride-contaminated concrete and in chloride-free concrete. The presence of chloride ion near the rebars changes the rest potentials of the rebars, and the difference in the rest potentials of the rebars leads to the galvanic corrosion cell in concrete (15). Large areas of the rebars in chloride-free concrete and exposure of the rebars to oxygen or air further accelerates the galvanic corrosion. Also, galvanic corrosion cells may

be developed by contact of different grades of materials as well as metallurgical defects in rebars (14).

1. Chloride Concentration and Distribution in Concrete

Chloride contents of concrete are usually measured by dry drilling and chemical analysis of the drilled samples. However, the conventional method does not provide any information on chloride distribution. A visualization technique involving color mapping was developed for the determination of chloride ion distribution and concentration near the reinforcement in concrete.

Chloride ion concentration in aqueous solutions can be determined by titration with mercuric nitrate in the presence of diphenylcarbazone as an indicator (16). This method was adapted to this investigation. Chloride ion on the concrete block surface reacted with mercuric ion to form insoluble mercuric chloride. Excess mercuric ion produced violet color when the diphenylcarbazone solution was sprayed over the filter paper as follows:

$$Hg^{++} + 2\ Cl^{-} \rightarrow HgCl_2 \qquad (1)$$

$$\text{Excess } Hg^{++} + \text{diphenylcarbazone} \rightarrow \text{violet color} \qquad (2)$$

The color map of Figure 1(b) shows the chloride ion distribution and concentration in the concrete. The light area indicates where chloride ion is present, and the different shades of purple represent chloride ion concentration which may be estimated from the calibration strips shown in Figure 1(c). The technique is simple and rapid for the determination of chloride ion concentration and its distribution in concrete.

2. Electrochemical Measurement Techniques for Rebar Corrosion

The galvanic current measurement method used in this investigation (Figure 2(a)), demonstrated that a chloride ion concentration difference generated a galvanic corrosion cell between a rebar in chloride-contaminated and another rebar in chloride-free concrete, and that the corrosion rates of the rebars in chloride-contaminated concrete increased with increasing chloride ion concentration. The corroded surfaces of rebars tested by galvanic current measurements suggested that localized corrosion was initiated at metallurgical defect areas. Metallurgical defects could be multi-phase microstructure, localized plastic deformation, welded joints, grain boundaries of microstructure, and non-metallic inclusions (17-19).

In the present investigation, the effect of chloride ion concentration on rebar corrosion in concrete was investigated by simulating the concrete environment by saturating the test solutions with concrete chips. To test the relevance of this simple laboratory experimental set-up, shown in Figure 2(a), the results were compared with those obtained in another experimental set-up as shown in Figure 2(b). The results shown in Figure 8(a) demonstrated that the shapes of galvanic currents were similar, and the galvanic currents eventually approached each other. The comparison suggested that the laboratory scale test may be used as a quick screening method to study the environmental parameters of rebar corrosion. The difference in the early stages of corrosion may be attributable to the slow diffusion of chloride ion through the concrete block. The diffusion rate of chloride ion through the concrete block was estimated by using Fick's second law of diffusion,

$$\frac{dc}{dt} = D \frac{d^2c}{dx^2} \tag{3}$$

$$c/c_e = 1 - erf\left(\frac{x}{2\sqrt{Dt}}\right) \tag{4}$$

where c is the concentration of chloride ion at a distance from the concrete surface, $x$, at a time, t, and $c_e$ is the concentration at equilibrium. Diffusion coefficient, D, of chloride ion through sound concrete was reported to be $10^{-7}$ - $10^{-8}$ $cm^2/sec$ (20). The distance from the concrete surface to the rebar (Figure 2(b)) was 2.8 cm. Well over ten years would be required for chloride ion to reach the rebar surface by diffusion through the concrete block tested (Figure 8(b)), but the experimental data in Figure 8(a) took only 0.25 year (90 days). Perhaps, micro-cracks in the concrete block might have facilitated the diffusion of chloride ion by an order of magnitude.

The surfaces of rebar samples tested by the electrochemical measurements (Figure 7) indicated that the rebars in chloride solutions acted as anodes, and those without chloride ions acted as cathodes. The cathode samples were seen to be free of corrosion which suggested that the rebar pairs in this investigation indeed acted as galvanic couples.

## 3. Mechanisms of Rebar Corrosion

Various corrosion products of the rebars have larger specific volumes than the rebar material itself. An increase in volume of the corrosion products causes stresses that can lead to cracks in concrete. These cracks allow easier penetration of chloride ions, and, therefore, more rapid attack on the rebars in concrete.

Corrosion of rebars in concrete may proceed by the formation of hydrated oxides. The reactions of corrosion can be expressed as

$$\tfrac{1}{2}\, O_2 + H_2O + 2e \rightarrow 2\, OH^- \qquad \text{(cathode)} \qquad (5)$$

$$Fe \rightarrow Fe^{++} + 2e \qquad \text{(anode)} \qquad (6)$$

The foregoing reaction products lead to the precipitation of hydroxides according to

$$Fe^{++} + 2\, OH^- \rightarrow Fe\,(OH)_2 \qquad (7)$$

$$2\, Fe\,(OH)_2 + \tfrac{1}{2}\, O_2 + H_2O \rightarrow 2\, Fe\,(OH)_3 \qquad (8)$$

The hydrated oxides in concrete can convert to various oxide species, such as magnetite ($Fe_3O_4$), hematite ($Fe_2O_3$), and goethite (FeOOH), leading to a complex system of compounds depending on pH, oxygen availability and the composition of rebars (21). FeOOH is more adherent to metal substrates than $Fe_2O_3$ and $Fe_3O_4$ (22), and, therefore, could slow the corrosion rates at the interface between the oxides and the metal matrix. The oxides shown in Figure 4(e) are suspected to be either $Fe_3O_4$ or $Fe_2O_3$.

Mechanical stresses are responsible for the cracks within corroded rebars. Sharp cracks were formed in the brittle rust by the fatigue stresses of road vibrations as shown in Figure 4(a). Irregular cracks in the metal matrix (Figure 4(b)) were presumably initiated by the corrosion attack and propagated by fatigue stresses (12).

From the corrosion point of view, welding is a particularly troublesome treatment. Because welding involves local heating of a material, it can lead to phase transformation, formation of secondary precipitates like inclusions, and the stress in and around the weld (23), which lead to significant local differences in electrochemical properties. Welded rebar experienced metallurgical transformations across the weld metal and the heat-affected zone so that the microstructures and morphologies became important factors to the

electrochemical characteristics. A wide range of microstructures could be developed based on cooling rates, and the microstructures depend on energy input, preheat, and weld bead size. As a result of different chemical compositions and weld inclusions (oxides and sulfides), the weld metal microstructures are usually significantly different from those of the heat-affected zone and the base metal (24). Accordingly, the electrochemical characteristics of the weld metal, heat-affected zone and base metal are different. It is apparent that the weld metal was more active than the base metal, and acted as an anode (Figure 9). Severe localized corrosion near the welded rebar is shown in Figure 3(e).

Plastic deformation occurred on the rebar as a result of slip when the rebar was bent plastically. The bending of rebars can be explained in terms of the dislocation theory. Dislocations are nucleated, rearranged, and accumulated around the plastically deformed area as the stresses are applied. The areas with a high density of dislocations are generally unstable thermodynamically and in a high energy state (10), which means electrochemically active. Difference in the electrochemical properties between high and low dislocation density areas accounts for the higher corrosion rate of the plastically bent rebar compared to the normal rebar as shown in Figure 9.

4. Retardation of Rebar Corrosion

Possible method of corrosion retardation by chemical additives to salt is shown schematically in Figure 12. The additives can have properties combining a corrosion inhibitor and a surfactant that imparts water-repellent coating on concrete would retard the penetration of salt solutions through pores and cracks in concrete, and even when the salt solution reaches the rebar, the surfactants adsorb on the rebar surface and act as corrosion

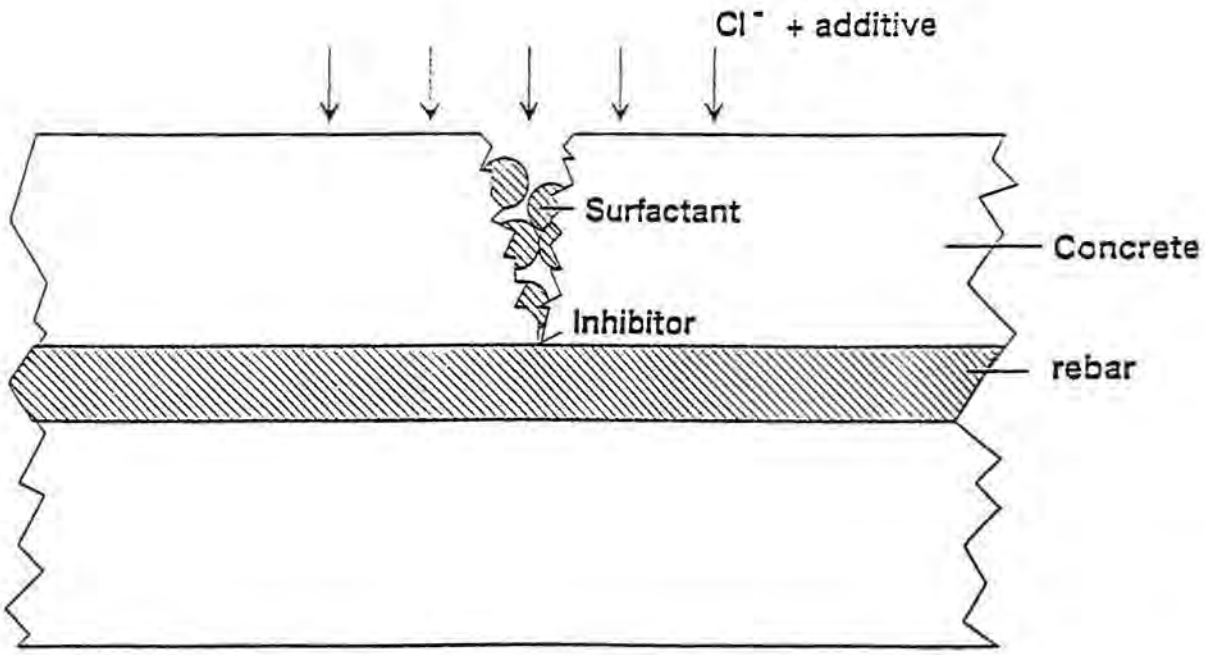


Figure 12. Schematic diagram for a possible method of corrosion retardation by chemical additives to salt.

inhibitors. Figures 10 and 11 indicated that the additives tested had the combined properties of a corrosion inhibitor and a surfactant.

The additives were organic compounds, which have different number of carbons and different hydrocarbon chainlengths. Further investigation is necessary to explore the optimum structure and chain length of those compounds for inhibitor activities on rebars and surface activities on concrete.

## CONCLUSIONS

1. Galvanic current measurement technique was developed for investigating the effects of chloride ion concentration on the rebar corrosion in simulated concrete conditions.
2. Visualization technique for estimating chloride concentration and distribution in concrete was developed.
3. Galvanic currents increased with increasing chloride ion concentration until visible yellow corrosion products appeared.
4. Galvanic currents of rebars measured in a simulated concrete solution correlated well with those of rebars imbedded in a concrete block.
5. Corrosion rates of welded and bent rebars determined by the galvanic current measurement method were about two orders of magnitude higher than those of normal rebars.
6. Severe localized corrosion was found near the grid-intersections, material defects, and welded areas of rebars in concrete.

7. Corrosion of rebars was initiated and propagated along the grain boundaries of rebar materials.

8. The pearlite structure of rebar microstructure was attacked preferentially to the ferrite structure under corrosive conditions in concrete.

9. Organic compounds slowed the corrosion of rebars acting as an adsorption-type inhibitor.

10. Organic compounds developed hydrophobic surfaces on concrete. Such an observation implies that salt solution may be prevented from penetrating microcracks in concrete.

## REFERENCES


1. S. Popovics, T. Simeonov, G. Bozhinov and N. Barovsky, "Durability of Reinforced Concrete in Sea Water," proceeding of conference 'Corrosion of Rebar in Concrete Construction', London, England, 13-15 June, 1983, pp. 233-237.

2. R. Driver and R.J. Meakins, "Effect of Sulfide Oxide on Inhibition of Acid Corrosion of Mild Steel and Pure Iron," British Corrosion Journal, 12, 1977, 115-117.

3. C. Andrade, V. Castelo, C. Alonso and J.A. Gonzalez, "The Determination of the Corrosion Rate of Steel Embedded in Concrete by the Polarization Resistance and AC Impedance Methods," Corrosion Effect of Stray Currents and the Techniques for Evaluating Corrosion of Rebars in Concrete, ASTM STP 906, 1986, pp. 43-63.

4. Kyosti Tuutti, "Corrosion of Steel in Concrete," Research Report of the Swedish Cement and Concrete Research Institute at the Institute of Technology, Stockholm, 1982.

5. L.M. Callow, I.A. Richardson and J.L. Dawson, "Corrosion Monitoring Using Polarization Resistance Measurement," British Corrosion Journal, 11, 1976, 132-139.

6. R. Driver and R.J. Meakins, "Electrochemical and Weight Loss Measurements of Inhibition of the Acid Corrosion of Steel," British Corrosion Journal, 9, 1974, 227-232

7. J.J. Pavlica, "Electrochemistry of Pyrrhotite in Flotation," M.S. Thesis, University of Minnesota, 1974.

8. R.L. Pozzo and I. Iwasaki, "Pyrite-Pyrrhotite-Grinding Media Interactions and Their Effects on Media Wear and Flotation," J. of Electrochemistry Society, 136, 1989, 1734-1740.

9. J.W. Jang, I. Iwasaki and J.J. Moore, "The Effect of Galvanic Interaction between Martensite and Ferrite in Grinding Media Wear," Corrosion, 45, 1989, 402-407. See also Corrigenda in Corrosion (in press).

10. G.P. Ray and R.A. Jarman, "Effect of Non-Metallic Inclusions on the Corrosion Fatigue of Mild Steel," British Corrosion Journal, 15, 1980, 226-227.

11. J.W. Jang and I. Iwasaki, "Rebar Corrosion Under Simulated Concrete Conditions Using Galvanic Current Measurement," 70th Annual Meeting of the Transportation Research Board, Washington, D.C., January, 1991, preprint 910155.

12. Metal Handbook, 8th Edition, ASM, vol. 9, 1974, pp. 68-78.

13. Z. Foroulis and H. Uhlig, "Effect of Impurities in Iron on Corrosion in Acids," Journal of Electrochemical Society, 112, 1965, 1177-1181.

14. H.H. Uhlig and R.W. Revie, Corrosion and Corrosion Control, John Wiley and Sons, Third Edition, 1985, pp. 114-121.

15. M.G. Fontana and N.D. Greene, Corrosion Engineering, McGraw-Hill, 1978, pp. 297-324.

16. D.F. Boltz and J.A. Howell, Calorimetric Determination of Nonmetals, John Wiley & Sons, Second Edition, 1978, pp. 92-97.

17. W.F. Savage, E.F. Nippes and F.F. Szekeres, "A Study of Weld Interface Phenomena in a Low Alloy Steel," Welding Journal, 55, September, 1976, 260S-268S.

18. J. Jang and J.E. Indacochea, "Inclusion Effects on Submerged-Arc Weld Microstructure," Journal of Materials Science, 22, 1987, 689-700.

19. C.S. Hartley and M.A. Eisenberg, "Phenomenological Plasticity and Dislocation Models of Deformation," proceedings of the International Conference, 'Dislocation Modelling of Physical Systems', Gainesville, Florida, June 22-27, 1980, pp. 373-380.

20. T. Miyagawa, "Corrosion and Protection of Reinforcing Steel in Concrete," Iron and Steel Institute of Japan, 76, 1990, 1449-1457.

21. T. Misawa, K. Hashimoto, W. Suetaka and S. Shimodaira, "Mechanism of Formation of Iron Oxide and Oxyhydroxides in Aqueous Solutions," proceedings of the Fifth International Congress on Metallic Corrosion, National Association of Corrosion Engineers, 1972, pp. 775-779.

22. J. Keiser, C. Brown and R. Heidersbach, "Characterization of the Passive Film Formed on Weathering Steels," Corrosion Science, 23, 1983, 251-259.

23. T.P. Hoar, "Corrosion Control at Weld Joints in Constructional Steels," British Corrosion Journal, 2, 1967, 46-48.

24. M. Henthorne and R.N. Parkins, "Some Aspects of the Influence of Structure upon Stress-Corrosion Cracking and Grain Boundary Corrosion in Mild Steel," British Corrosion Journal, 2, 1967, 186-192.

# APPENDIX I

Paper No. 91 0 1 5 6

# PREPRINT

**Title:** Visualization of Chloride Distribution in Concrete.

**Author(s):** J.W. Jang and I. Iwasaki

Transportation Research Board
70th Annual Meeting
January 13-17, 1991
Washington, D.C.

# VISUALIZATION OF CHLORIDE DISTRIBUTION IN CONCRETE

An Abridgment Submitted to

Transportation Research Board
2101 Constitution Avenue, N.W.
Washington, D.C. 20418

by

J.W. Jang, Research Associate
and
I. Iwasaki, Professor

Mineral Resources Research Center
University of Minnesota
Minneapolis, MN 55455
612-625-3344
(FAX) 612-625-1882

# VISUALIZATION OF CHLORIDE DISTRIBUTION IN CONCRETE

**J.W. Jang and I. Iwasaki**
**Mineral Resources Research Center**
**University of Minnesota**
**Minneapolis, MN 55455**

## ABSTRACT

Chloride contents of concrete are usually measured by dry drilling and chemical analysis of the drilled samples. However, the conventional method does not provide any information on chloride distribution. A visualization technique involving color mapping was developed for the determination of chloride ion distribution and concentration near the reinforcement in concrete.

## INTRODUCTION

Localized corrosion of reinforcements in concrete is caused by the impurities of the reinforcement material, deformation of the reinforcement surfaces, concentration difference of chloride ion near the reinforcement, and the complex interactions of the above factors (1, 2). Deformed and/or defect surfaces of reinforcements could be the corrosion initiation sites even under very low chloride ion concentrations because of their thermodynamic instabilities, while no corrosion may be found on the deformation-free and/or defect-free surfaces under relatively high chloride ion concentrations. Galvanic interactions between corroding and non-corroding areas accelerate the localized corrosion at the surfaces of reinforcements.

Similarly, the concentration differences of chloride ion near reinforcements create galvanic cells between the high and low or no chloride concentration surfaces of the reinforcements (2). High chloride concentration areas become the anode, and low or no chloride concentration areas the cathode. Corrosion rates increase as the chloride concentration difference increases.

Chloride contents of concrete are usually measured by dry drilling and chemical analysis of the drilled samples. However, the conventional method does not provide any information on chloride distribution near the reinforcement in concrete, particularly along hair-line cracks. Such an information would be essential in understanding the localized corrosion mechanisms and kinetics.

The purpose of this note is to communicate a visualization technique in use in our

laboratory for the determination of chloride ion distribution and concentration near the reinforcements in concrete.

## EXPERIMENTAL

Concrete blocks containing reinforcements were collected in the field, cut and ground to expose flat smooth surfaces. The concrete surfaces were finished with 320 grit silicon carbide abrasive papers. A crack was intentionally made from one edge of the concrete block to the reinforcement as shown in Figure 1 (a). A solution of 10% $CaCl_2$ was applied repeatedly to the crack in order to simulate the chloride penetration through the crack.

The indicator solutions used for detection and determination of chloride ion on the surface of the concrete block were 0.025% mercuric nitrate in 0.008M nitric acid, and 0.25% diphenylcarbazone in methanol. A filter paper was wetted by the mercuric nitrate solution uniformly. The filter paper was placed over the flat smooth concrete block, pressed firmly with a roller and left standing for a few minutes. Then the filter paper was peeled off and the diphenylcarbazone solution was sprayed over it, and air dried. For the purpose of calibration, 0, 0.01, 0.1, 1, and 10% $CaCl_2$ solutions were also applied to filter papers, and the color was developed as before.

## RESULTS AND DISCUSSION

Chloride ion concentrations in aqueous solutions can be determined by titration with mercuric nitrate in the presence of diphenylcarbazone as an indicator (3). This method was adapted to this investigation. Chloride ion on the concrete block surface reacted with mercuric ion to form insoluble mercuric chloride. Excess mercuric ion produced violet color

when the diphenylcarbazone solution was sprayed over the filter paper as follows:

$$Hg^{++} + 2\,Cl^{-} \rightarrow HgCl_2$$

$$\text{Excess } Hg^{++} + \text{diphenylcarbazone} \rightarrow \text{violet color}$$

The color map of Figure 1 (b) shows the chloride ion distribution and concentration in the concrete. The light area indicates where chloride ion is present, and the different shades of purple represent chloride ion concentrations which may be estimated from the calibration strips shown in Figure 1 (c). The technique is simple and rapid for the determination of chloride ion concentration and its distribution in concrete.

## ACKNOWLEDGEMENT

The authors express appreciation to the Center for Transportation Studies at the University of Minnesota for support of this research.

## REFERENCES

1. G.P. Ray and R.A. Jarman, "Effect of Non-Metallic Inclusions on the Corrosion Fatique of Mild Steel," British Corrosion Journal, 15, 1980, 226-227.
2. J.W. Jang and I. Iwasaki, "Rebar Corrosion Under Simulated Concrete conditions Using Galvanic Current Measurement," 70th Annual Meeting of the Transportation Research Board, Washington, D.C., January, 1991, preprint 910155.
3. D.F. Boltz and J.A. Howell, Colorimetric Determination of Nometals, John Wiley & Sons, Second Edition, 1978, pp. 92-97.

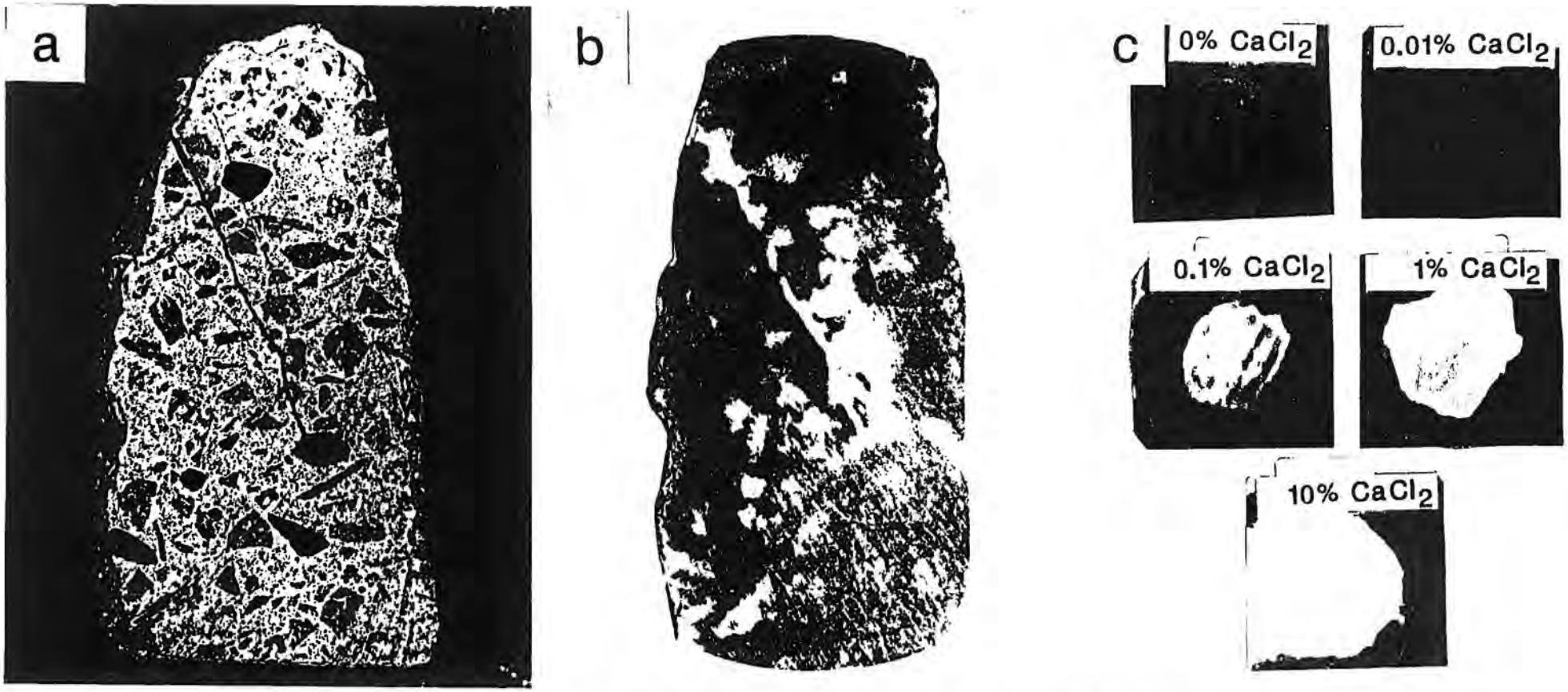


Figure 1. Visualization results for chloride ion distribution and concentration in concrete; (a) concrete sample with rebar, (b) color map and (c) calibration strips.

# APPENDIX II

Paper No. 91 0 1 5 5

# PREPRINT

**Title:** Rebar Corrosion under Simulated Concrete Conditions using Galvanic Current Measurements.

**Author(s):** J.W. Jang and I. Iwasaki

Transportation Research Board
70th Annual Meeting
January 13-17, 1991
Washington, D.C.

# REBAR CORROSION UNDER SIMULATED CONCRETE CONDITIONS USING GALVANIC CURRENT MEASUREMENTS

A Paper Submitted to

Transportation Research Board
2101 Constitution Avenue, N.W.
Washington, D.C. 20418

by

J.W. Jang, Research Associate
and
I. Iwasaki, Professor

Mineral Resources Research Center
University of Minnesota
Minneapolis, MN 55455
612-625-3344
(FAX) 612-625-1882

# REBAR CORROSION UNDER SIMULATED CONCRETE CONDITIONS USING GALVANIC CURRENT MEASUREMENTS

J.W. Jang and I. Iwasaki
Mineral Resources Research Center
University of Minnesota
Minneapolis, MN 55455

## ABSTRACT

A galvanic current measurement method was developed as a rapid and simple technique to study the effect of chloride concentration, welding and bending on the rebar corrosion in concrete. Some parameters that were responsible for the corrosion of rebar were identified by using the galvanic current measurement method as well as optical and scanning electron microscopy. Examination of corroded rebars collected from the field showed severe localized corrosion near grid-intersections, material defects and welded areas in concrete, and preferential corrosion attacks on certain micro-constituents of the rebar material. The corrosion behaviors of the field samples are discussed in the light of the galvanic current measurement results.

## INTRODUCTION

The main factors that influence the initiation and propagation of rebar corrosion in concrete are concrete properties, aggressive corrosion elements from the environment and concrete, and defects of the reinforcing material. The presence of chloride ion appears to be the dominant cause for rebar corrosion in concrete.

The electrochemical corrosion in concrete may occur because of the non-uniformities of the reinforcing steel (different steels, welds, active sites on the steel surface) (1), or of chemical or physical environments in the surrounding concrete (2). These non-uniformities under certain specific conditions can produce significant electric potential differences and resultant corrosion. Macro-cell corrosion in rebars due to the difference in chloride ion concentration, the structural and compositional defects of rebars in concrete could accelerate the localized corrosion.

Rebar corrosion is complex and the basic mechanisms of individual factors are not well understood because of the complex nature of the physical and electrochemical factors and because of their interdependence. Many research efforts (3,4) have been made in the last two decades which contributed to the understanding of rebar corrosion, to the developments of monitoring methods and to the protection methods of rebars. However, many contradictory experimental results and views have been reported on the deterioration behavior of reinforced concrete structures.

Corrosion rates of rebars can be determined by measuring weight losses only after the concrete structure is destroyed. Since the corrosion of rebar is electrochemical in nature, many approaches (5,6) have been tried to develop electrochemical methods for testing. However, various fundamental and experimental factors contribute to the

inaccuracies in these results. The linear polarization and polarization resistance techniques of monitoring corrosion rates in concrete has uncertain factors such as the location of counter and reference electrodes and the material of the counter electrode (5). In addition, these techniques are not applicable for a continuous monitoring of corroding rebars in situ over extended periods of time, while a galvanic current measurement technique is capable of such measurements. The method has been used successfully in an investigation on the corrosion mechanism of grinding media under dynamic conditions in our laboratory for the past 15 years (7-9).

The purpose of the present investigation was to develop a galvanic current measurement technique for estimating the corrosion rates of rebars in simulated concrete environments and for investigating the effects of relevant parameters that may be responsible for macro-cell corrosion on rebars as a function of chloride ion concentration.

## EXPERIMENTAL

### Electrochemical Measurements

A galvanic current measurement method was chosen for investigating the effect of chloride ion concentration on rebar corrosion in concrete. A laboratory galvanic cell was made by dipping two rebars in chloride-containing and chloride-free solutions and short-circuiting them, as shown in Figure 1(a). The test solutions were prepared by saturating 500 ml deionized water with 25g of concrete chips of approximately 1/8" in size in a series of 600 ml beakers and adding 0, 0.1, 1 and 10% calcium chloride in one set of beakers and none in the other set in order to simulate the chemistry of concrete environment. The pH of the concrete chip saturated solution was 12. 5. To compensate for the evaporation loss,

the solution levels were maintained constant by frequent addition of distilled water. The chemical composition of the rebars was determined by spectrographic analysis as follows:

| C | Mn | P | S | Si | Sn | Cu | Ni | Cr | Mo |
|---|---|---|---|---|---|---|---|---|---|
| 0.35 | 0.72 | 0.021 | 0.053 | 0.03 | 0.009 | 0.04 | 0.04 | 0.05 | 0.10 |

The ½" rebar samples were made into electrodes by attaching an electrical wire to ¼" high steel pieces with a silver conductive epoxy and by mounting in epoxy. After the epoxy hardened, the bottom surfaces of the mounted rebars were ground and polished. A Lucite tube of ¼" I.D. was attached to the other flat surface by using 5-minute epoxy.

To test the relevance of the foregoing beaker-scale method, galvanic current measurements were made between two rebars imbedded in a concrete block obtained from the field. The concrete block had an overall dimension of 2.0 x 5.0 x 2.5 inch, and the ½ inch diameter rebars were imbedded 2 inches apart. The concrete was analyzed to contain approximately 1100 ppm $Cl^-$. The concrete block was divided into two sides with a barrier as shown in Figure 1(b). One side was filled with 10% $CaCl_2$ solution and the other filled with deionized water. The rebars were short-circuited and the galvanic currents between the two were monitored as a function of time.

The effects of welded and bent rebars on galvanic corrosion in concrete was investigated by using a galvanic cell mentioned earlier (Figure 1 (a)) by dipping and short-circuiting normal and welded or bent rebars in 10% $CaCl_2$ solution saturated with concrete chips as described earlier in an attempt to simulate the concrete environment. Localized

strain of a bent rebar was induced by a three point loading. The bend angle of the ½ inch diameter rebar was approximately 30°. A welded sample also was prepared by a shield-metal arc welding method. The weld was made on a ½" diameter rebar using Lincoln E7024 flux electrode and d.c. straight polarity with a Miller model 330A/BP welding machine. The welded rebar sample was ground to a smooth surface after the slag was removed.

All the measurements were made with an EG & G model 350 A corrosion measurement console. A saturated calomel electrode (SCE) was used as the reference electrode via a salt bridge containing a saturated solution of ammonium nitrate.

Field Samples

Rebar samples with and without concrete blocks were collected from the I-94 bridge deck in front of the State Capital, St. Paul and the I-94 Lowry Hill Tunnel pavement in Minneapolis, Minnesota. The diameter of the rebars was ½ inch, and the chloride content in concrete analyzed 1100 ppm. The rebars were examined for corrosion behavior and corrosion initiation sites through observation of the surfaces under a JEOL 840 II scanning electron microscope and the cross section by an Olympus microscope model PM-10AD.

The rebar samples for scanning electron microscopy were cleaned by dipping in 10% hydrochloric acid for 5 seconds and by rinsing with distilled water. The rinsed samples were dried with 99% isopropyl alcohol and blowing air over them.

The cross-cut rebars were cold-mounted in epoxy and polished using conventional metallographic polishing techniques and etched with 2% Nital solution.

## RESULTS

Galvanic Current Measurements

Combination potentials and galvanic currents of rebars were obtained at different chloride ion concentrations as a function of time by using the galvanic current measurement method shown in Figure 1(a), and the results are presented in Figure 2. The galvanic currents increased with increasing chloride ion concentration until visible yellow corrosion products appeared on the rebar sample surfaces as indicated by arrows in Figure 2(a). After the corrosion products appeared, the galvanic currents increased dramatically in 0, 0.1 and 1% $CaCl_2$ solutions. In 10% $CaCl_2$ solution, the galvanic current increased and then decreased when the corrosion products appeared. The combination potentials were most active in 10% $CaCl_2$, followed by 1, 0, and 0.1% $CaCl_2$. The combination potentials are seen to cross over randomly after 100 days as shown in Figure 2(b).

The surfaces of rebar samples were examined for their corrosion behaviors after completing the galvanic current measurements. The results are shown in Figure 3. The left-side photos show the surfaces of rebar samples recovered from the solutions containing chloride ion, while the right-side photos are from the chloride-free solutions. The yellow corrosion products on the rebar samples can be seen only in the left-side photos. The rebar samples in the chloride solutions acted as anodes and those in the chloride-free solutions acted as cathodes. It is apparent that those samples which acted as cathodes (right-side photos) are all free of rust. The figure also shows that the corroded areas on the surfaces of rebar samples increased with increasing chloride ion concentration in the solution, and hence with increasing galvanic currents.

The galvanic currents of rebars imbedded in a concrete block (Figure 1(b)) were

measured and the results are shown in Figure 4. The galvanic currents decreased initially, and then increased. After 50 days, the galvanic currents decreased, and eventually approached the galvanic currents obtained in the simulated concrete environments (Figure 1 (a)).

The galvanic currents of the normal, bent and welded rebars were obtained by using the galvanic cell (Figure 1 (a)) as a function of time and the results are plotted in Figure 5. The galvanic currents of bent and welded rebars decreased with time, and those of normal rebar decreased initially, then increased somewhat and remained constant thereafter. Note that the galvanic currents of welded and bent rebars were two orders of magnitude higher than those of normal rebar.

Optical and Scanning Electron Microscope Observations of Corroded Rebar.

Figure 6(a and b) show typical field samples of corroded rebars in concrete with yellow stains of corrosion products and concrete cracks by the corroded rebars. Severe localized corrosion of the rebars was found near grid-intersections (Figure 6(c)), material defects (inclusions) (Figure 6(d)) and welded areas (Figure 6(e)). Figure 6(f) shows that the rebar lost more than a half of the volume from the original rebar by corrosion.

The surfaces of corroded rebars were examined under a scanning electron microscope. Figure 7 shows numerous sharp cracks on the rust layer (a) and irregular cracks on the rebar metal matrix (b). The micrographs (Figure 7(c) and (d)) of corroded rebar surfaces indicate that the corrosion of rebars was initiated and propagated along the grain boundaries of the rebar material microstructure, especially carbide (cementite). Also, there was a space between the rust layer and the metal matrix (Figure 7(e)), which was large

enough for chloride ion to spread throughout the whole rebar. The parallel and continuous lines (striations) in Figure 7(f) suggest that the cracks on the oxide layer propagated by fatigue stresses due to vibration (10).

The corroded rebars were cut, and the cross sections examined under an optical microscope. Figures 8 (a) and (b) show that even though the surfaces of corroded rebars appeared smooth, severe corrosion was taking place underneath. Conventional rebar materials are mild steel, which consists of ferrite (white in Figure 8) and pearlite (dark) structures. Figure 8 (c) shows that the pearlite structure was attacked preferentially, and that the ferrite structure survived longer than the pearlite structure under corrosive conditions in concrete. Figure 8 (d) was obtained by using a polarized filter, which shows that the corrosion of the rebar propagated along the grain boundaries of the rebar material microstructures.

## DISCUSSION

Conventional rebar materials are mild steel. The usual impurities have no significant effect on the corrosion rate in atmosphere, neutral water, or soil, but have a marked effect in the case of acid and chloride attacks (11). The presence of sulfur in the form of inclusions markedly increases the rate of attack. Small additions of copper, chromium, and/or nickel (12), and the reduction of sulfur (inclusions) decrease the corrosion rates of rebars significantly in chloride environments.

Galvanic cells between dissimilar constituents (e.g., ferrite and pearlite) of a mild steel structure, and between constituents and inclusions along the grain boundaries could accelerate the rebar corrosion as shown in Figures 7 and 8. Differences in potentials

between the dissimilar constituents of the structure cause electron flow between them when they are electrically coupled (9). Direction of the current flow (galvanic behavior) depends on which constituent is more active. Thus, the more active constituent becomes the anode, and the more noble constituent becomes the cathode in the couple. The driving force for galvanic corrosion is the difference in potential between the constituents. Figure 8 (c) suggests that the pearlite was the anode and the ferrite was the cathode.

The use of deicing salts in winter could develop a strong galvanic corrosion cell between the rebars in chloride-contaminated concrete and in chloride-free concrete. The presence of chloride ion near the rebars changes the rest potentials of the rebars, and the difference in the rest potentials of the rebars leads to the galvanic corrosion cell in concrete (13). A large area of the rebar in chloride-free concrete and exposure of the rebar to oxygen or air further accelerates the galvanic corrosion. Also, galvanic corrosion cells may be developed by contact of different grades of materials as well as metallurgical defects in rebars(12).

The galvanic current measurement method used in this investigation (Figure 1(a)), demonstrated that a chloride ion concentration difference generated a galvanic corrosion cell between a rebar in chloride-contaminated and another rebar in chloride-free concrete, and that the corrosion rates of the rebars in chloride-contaminated concrete increased with increasing chloride ion concentration. The corroded surfaces of rebars tested by galvanic current measurements suggested that localized corrosion was initiated at metallurgical defect areas. Metallurgical defects could be multi-phase microstructure, localized plastic deformation, welded joint, grain boundaries of microstructure, and non-metallic inclusions(14-16).

In the present investigation, the effect of chloride ion concentration on rebar corrosion in concrete was investigated by simulating the concrete environment by saturating the test solutions with concrete chips. To test the relevance of this simple laboratory experimental set-up, shown in Figure 1 (a), the results were compared with those obtained in another experimental set-up as shown in Figure 1 (b). The results shown in Figure 4(a) demonstrated that the shapes of galvanic currents were similar, and the galvanic currents eventually approached each other. The comparison suggested that the laboratory scale test may be used as a quick screening method to study the environmental parameters of rebar corrosion. The difference in the early stages of corrosion may be attributable to the slow diffusion of chloride ions through the concrete block. The diffusion rate of chloride ion through the concrete block was estimated by using Fick's second law of diffusion,

$$\frac{dc}{dt} = D \frac{d^2c}{dx^2} \tag{1}$$

$$c/c_e = 1 - erf\left(\frac{x}{2\sqrt{Dt}}\right) \tag{2}$$

where c is the concentration of chloride ion at a distance from the concrete surface, $x$, at a time, t, and $c_e$ is the concentration at equilibrium. Diffusion coefficient, D, of chloride ion through sound concrete was reported to be $10^{-7}$ - $10^{-8}$ $cm^2/sec$ (17). The distance, from the concrete surface to the rebar (Figure 1 (b)) was 2.8 cm. Well over ten years would be required for chloride ion to reach the rebar surface by diffusion through the concrete block tested (Figure 4(b)), but the experimental data in Figure 4 (a) took only 0.25 year (90 days). Perhaps, micro-cracks in the concrete block might have facilitated the diffusion of chloride

ions by an order of magnitude.

The surfaces of rebar samples tested by the electrochemical measurements (Figure 3) indicated that the rebars in chloride solutions acted as anodes, and those without chloride ions acted as cathodes. The cathode samples were seen to be free of corrosion which suggested that the rebar pairs in this investigation indeed acted as galvanic couples.

Various corrosion products of the rebars have larger specific volumes than the rebar material itself. An increase in volume of the corrosion products causes stresses that can lead to cracks in concrete. These cracks allow easier penetration of chloride ions, and, therefore, more rapid attack on the rebars in concrete.

Corrosion of rebars in concrete may proceed by the formation of hydrated oxides. The reactions of corrosion can be expressed as

$$\tfrac{1}{2}\, O_2 + H_2O + 2e \rightarrow 2\, OH^- \qquad \text{(cathode)} \qquad (3)$$

$$Fe \rightarrow Fe^{++} + 2e \qquad \text{(anode)} \qquad (4)$$

The foregoing reaction products lead to the precipitation of hydroxides according to

$$Fe^{++} + 2\, OH^- \rightarrow Fe\,(OH)_2 \qquad (5)$$

$$2\, Fe\,(OH)_2 + \tfrac{1}{2}\, O_2 + H_2O \rightarrow 2\, Fe\,(OH)_3 \qquad (6)$$

The hydrated oxides in concrete can convert to various oxide species, such as magnetite ($Fe_3O_4$), hematite ($Fe_2O_3$), and goethite (FeOOH), leading to a complex system of compounds depending on pH, oxygen availability and the composition of rebars (18). FeOOH is more adherent to metal substrates than $Fe_2O_3$ and $Fe_3O_4$ (19), and, therefore, could slow the corrosion rate at the interface between the oxides and the metal matrix. The oxides shown in Figure 7 (e) are suspected to be either $Fe_3O_4$ or $Fe_2O_3$.

Mechanical stresses are responsible for the cracks within the corroded rebar. Sharp

cracks were formed in the brittle rust by the fatigue stresses of road vibrations as shown in Figure 7 (a). Irregular cracks in the metal matrix (Figure 7(b)) were presumably initiated by the corrosion attack and propagated by fatigue stresses (10).

From the corrosion point of view, welding is a particularly troublesome treatment. Because welding involves local heating of a material, it can lead to phase transformation, formation of secondary precipitates like inclusions, and the stress in and around the weld (20), which lead to significant local differences in electrochemical properties. Welded rebar experienced metallurgical transformations across the weld metal and the heat-affected zone so that the microstructures and morphologies became important factors to the electrochemical characteristics. A wide range of microstructures could be developed based on cooling rates, and the microstructures depend on energy input, preheat, and weld bead size. As a result of different chemical compositions and weld inclusions (oxides and sulfides), the weld metal microstructures are usually significantly different from those of the heat-affected zone and the base metal (21). Accordingly, the electrochemical characteristics of the weld metal, heat-affected zone and base metal are different. The weld metal was more active than the base metal, and acted as an anode (Figure 5). Severe localized corrosion near the welded rebar is shown in Figure 6 (e).

Plastic deformation occurred on the rebar as a result of slip when the rebar was bent plastically. The bending of rebars can be explained in terms of the dislocation theory. Dislocations are nucleated, rearranged, and accumulated around the plastically deformed area as the stresses are applied. The areas with a high density of dislocations are generally unstable thermodynamically and in a high energy state (22), which means electrochemically active. Difference in the electrochemical properties between high and low dislocation

density areas accounts for the plastically bent rebars higher corrosion rate compared to the normal rebar as shown in Figure 5.

## CONCLUSIONS

1. Galvanic current measurements technique was developed for investigating the effects of chloride ion concentration on the rebar corrosion in simulated concrete conditions.
2. Galvanic currents increased with increasing chloride ion concentration until visible yellow corrosion products appeared.
3. Galvanic currents of rebars measured in a simulated concrete solution correlated well with those of rebars imbedded in a concrete block.
4. Corrosion rates of welded and bent rebars determined by the galvanic current measurement method were about two orders of magnitude higher than those of normal rebars.
5. Severe localized corrosion was found near the grid-intersections, material defects, and welded areas of rebars in concrete.
6. Corrosion of rebars was initiated and propagated along rebar material grain boundaries.
7. The pearlite structure of rebar microstructure was attacked preferentially to the ferrite structure under corrosive conditions in concrete.

## ACKNOWLEDGMENT

The authors express appreciation to the Center for Transportation Studies at the University of Minnesota for support of this research.

## REFERENCES

1. S. Popovics, T. Simeonov, G. Bozhinov and N. Barovsky, "Durability of Reinforced Concrete in Sea Water," proceeding of conference 'Corrosion of Rebar in Concrete Construction', London, England, 13-15 June, 1983, pp. 233-237.
2. R. Driver and R.J. Meakins, "Effect of Sulfide Oxide on Inhibition of Acid Corrosion of Mild Steel and Pure Iron," British Corrosion Journal, 12, 1977, 115-117.
3. C. Andrade, V. Castelo, C. Alonso and J.A. Gonzalez, "The Determination of the Corrosion Rate of Steel Embedded in Concrete by the Polarization Resistance and AC Impedance Methods," Corrosion Effect of Stray Currents and the Techniques for Evaluating Corrosion of Rebars in Concrete, ASTM STP 906, 1986, pp. 43-63.
4. Kyosti Tuutti, "Corrosion of Steel in Concrete," Research Report of the Swedish Cement and Concrete Research Institute at the Institute of Technology, Stockholm, 1982.
5. L.M. Callow, I.A. Richardson and J.L. Dawson, "Corrosion Monitoring Using Polarization Resistance Measurement," British Corrosion Journal, 11, 1976, 132-139.

6. R. Driver and R.J. Meakins, "Electrochemical and Weight Loss Measurements of Inhibition of the Acid Corrosion of Steel," British Corrosion Journal, 9, 1974, 227-232

7. J.J. Pavlica, "Electrochemistry of Pyrrhotite in Flotation," M.S. Thesis, University of Minnesota, 1974.

8. R.L. Pozzo and I. Iwasaki, "Pyrite-Pyrrhotite-Grinding Media Interactions and Their Effects on Media Wear and Flotation," J. of Electrochemistry Society, 136, 1989, 1734-1740.

9. J.W. Jang, I. Iwasaki and J.J. Moore, "The Effect of Galvanic Interaction between Martensite and Ferrite in Grinding Media Wear," Corrosion, 45, 1989, 402-407. See also Corrigenda in Corrosion (in press).

10. Metal Handbook, 8th Edition, ASM, vol. 9, 1974, pp. 68-78.

11. Z. Foroulis and H. Uhlig, "Effect of Impurities in Iron on Corrosion in Acids," Journal of Electrochemical Society, 112, 1965, 1177-1181.

12. H.H. Uhlig and R.W. Revie, Corrosion and Corrosion Control, John Wiley and Sons, Third Edition, 1985, pp. 114-121.

13. M.G. Fontana and N.D. Greene, Corrosion Engineering, McGraw-Hill, 1978, pp. 297-324.

14. W.F. Savage, E.F. Nippes and F.F. Szekeres, "A Study of Weld Interface Phenomena in a Low Alloy Steel," Welding Journal, 55, September, 1976, 260S-268S.

15. J. Jang and J.E. Indacochea, "Inclusion Effects on Submerged-Arc Weld Microstructure," Journal of Materials Science, 22, 1987, 689-700.

16. C.S. Hartley and M.A. Eisenberg, "Phenomenological Plasticity and Dislocation Models of Deformation," proceedings of the International Conference, 'Dislocation Modelling of Physical Systems', Gainesville, Florida, June 22-27, 1980, pp. 373-380.

17. T. Miyagawa, "Corrosion and Protection of Reinforcing Steel in Concrete," Iron and Steel Institute of Japan, 76, 1990, 1449-1457.

18. T. Misawa, K. Hashimoto, W. Suetaka and S. Shimodaira, "Mechanism of Formation of Iron Oxide and Oxyhydroxides in Aqueous Solutions," proceedings of the Fifth International Congress on Metallic Corrosion, National Association of Corrosion Engineers, 1972, pp. 775-779.

19. J. Keiser, C. Brown and R. Heidersbach, "Characterization of the Passive Film Formed on Weathering Steels," Corrosion Science, 23, 1983, 251-259.

20. T.P. Hoar, "Corrosion Control at Weld Joints in Constructional Steels," British Corrosion Journal, 2, 1967, 46-48.

21. M. Henthorne and R.N. Parkins, "Some Aspects of the Influence of Structure upon Stress-Corrosion Cracking and Grain Boundary Corrosion in Mild Steel," British Corrosion Journal, 2, 1967, 186-192.

22. G.P. Ray and R.A. Jarman, "Effect of Non-Metallic Inclusions on the Corrosion Fatigue of Mild Steel," British Corrosion Journal, 15, 1980, 226-227.

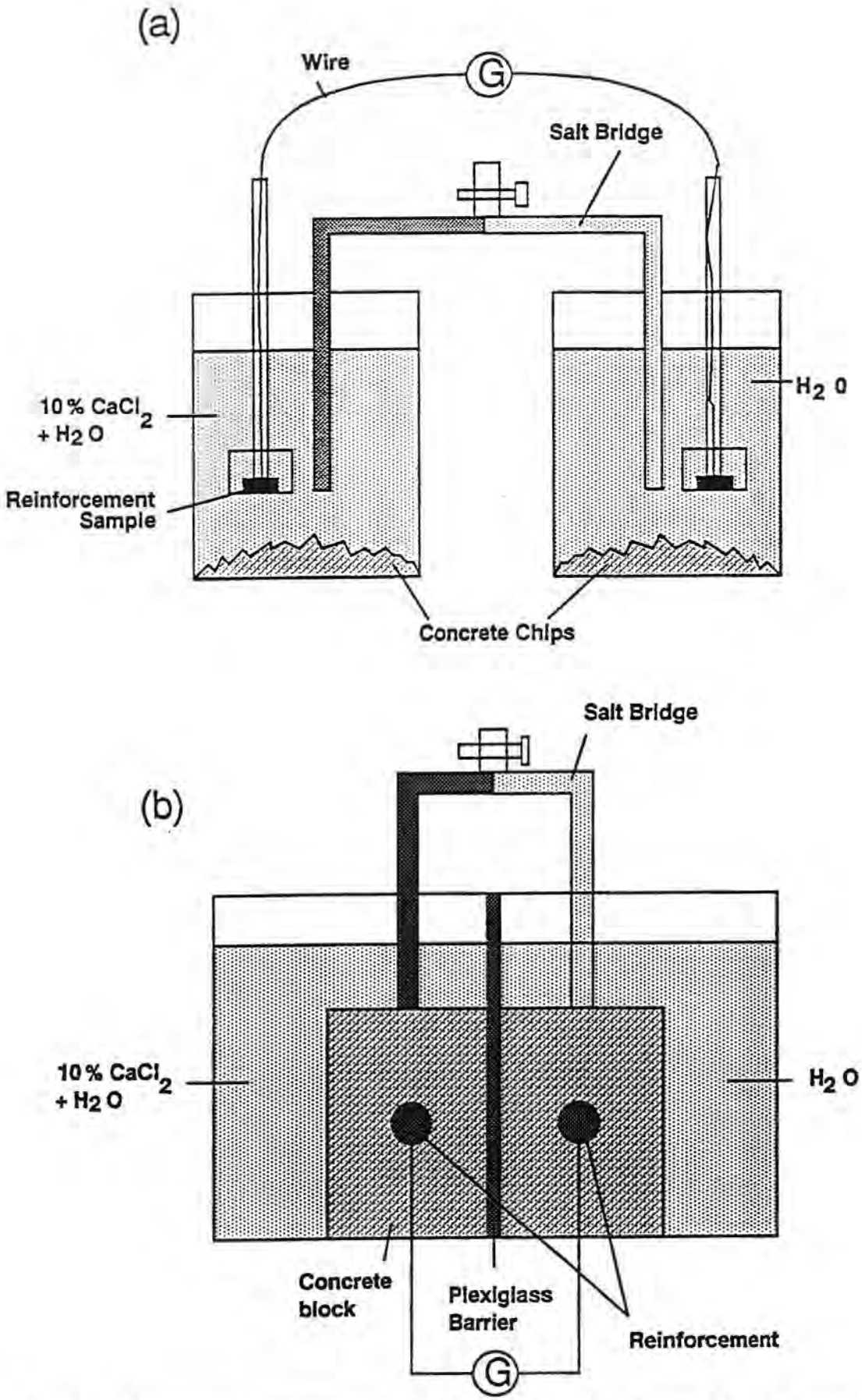


Figure 1. Schematic representation of experimental set-ups for galvanic current measurements of reinforcements in (a) a simulated concrete environment, and (b) a concrete block.

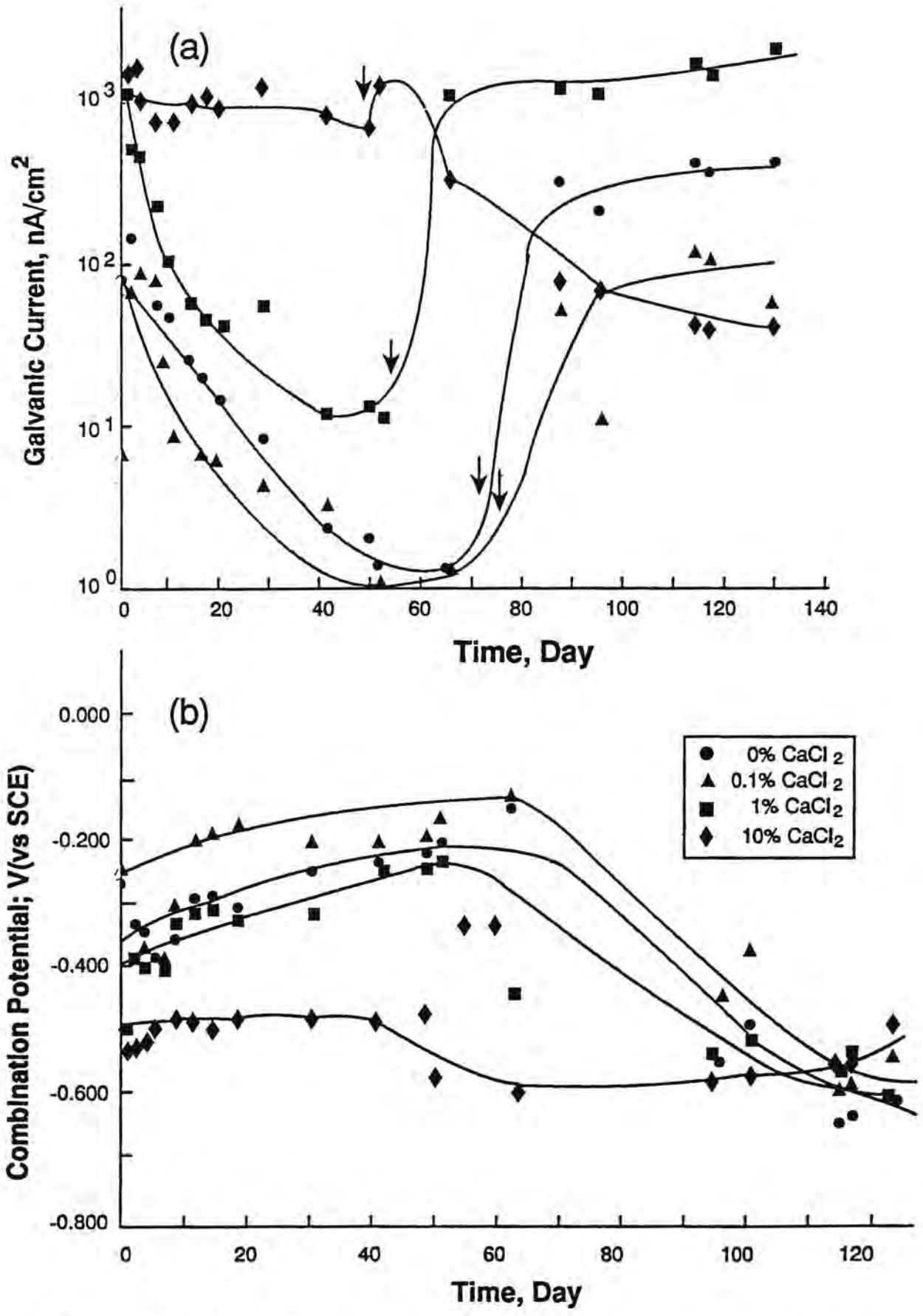


Figure 2. Galvanic current and combination potential as a function of time at different chloride concentrations.

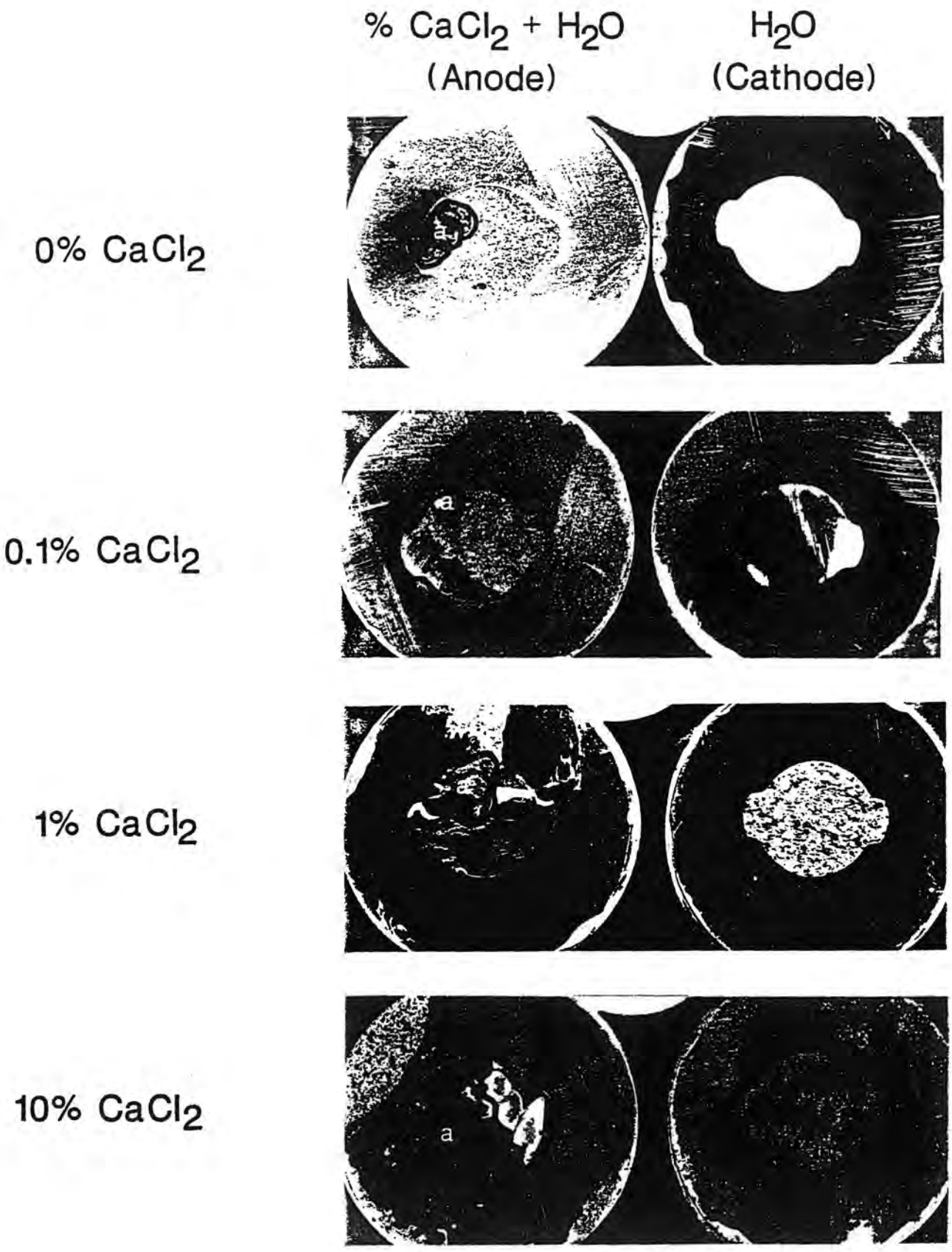


Figure 3. Corroded areas (indicated by **a**) on reinforcement surface showing the effect of chloride ion concentration.

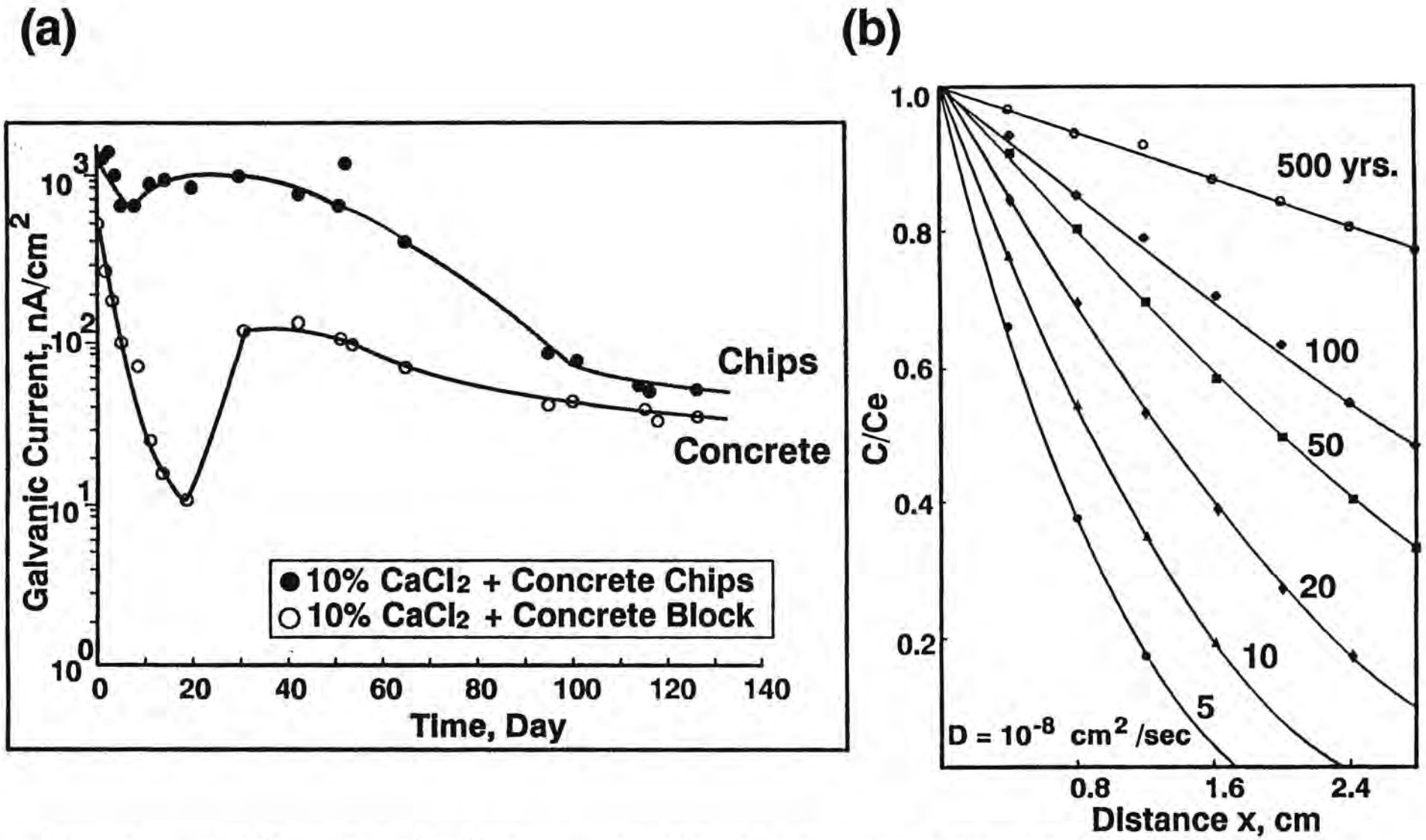


Figure 4. (a) Comparison of galvanic currents obtained by the concrete chip method (Figure 1(a)) and the concrete block method (Figure 1 (b)), and (b) chloride movement by diffusion as a function of distance from concrete surface to rebar (Equation (2)).

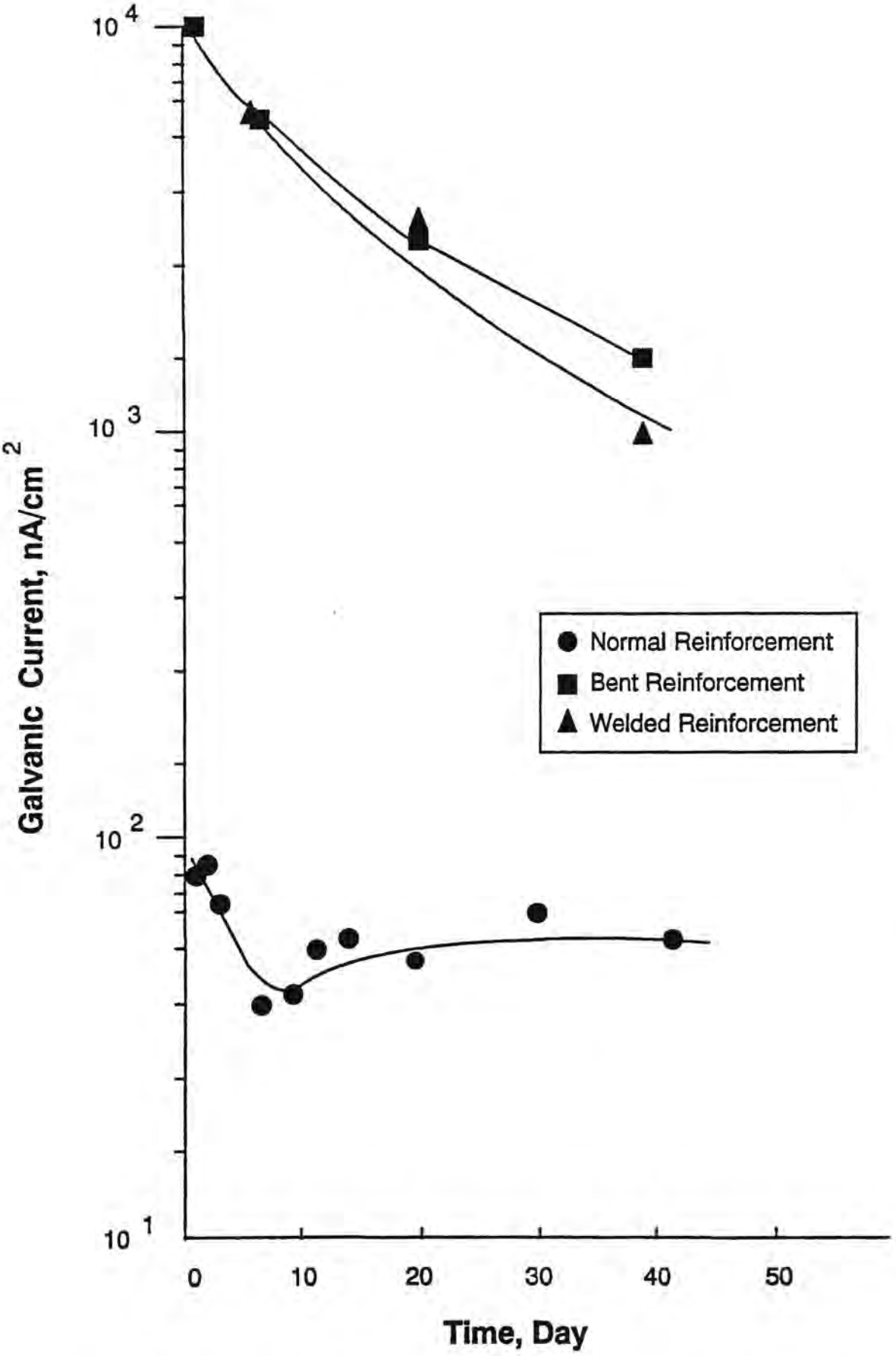


Figure 5. Effect of deformation and welding on galvanic corrosion currents of reinforcement.

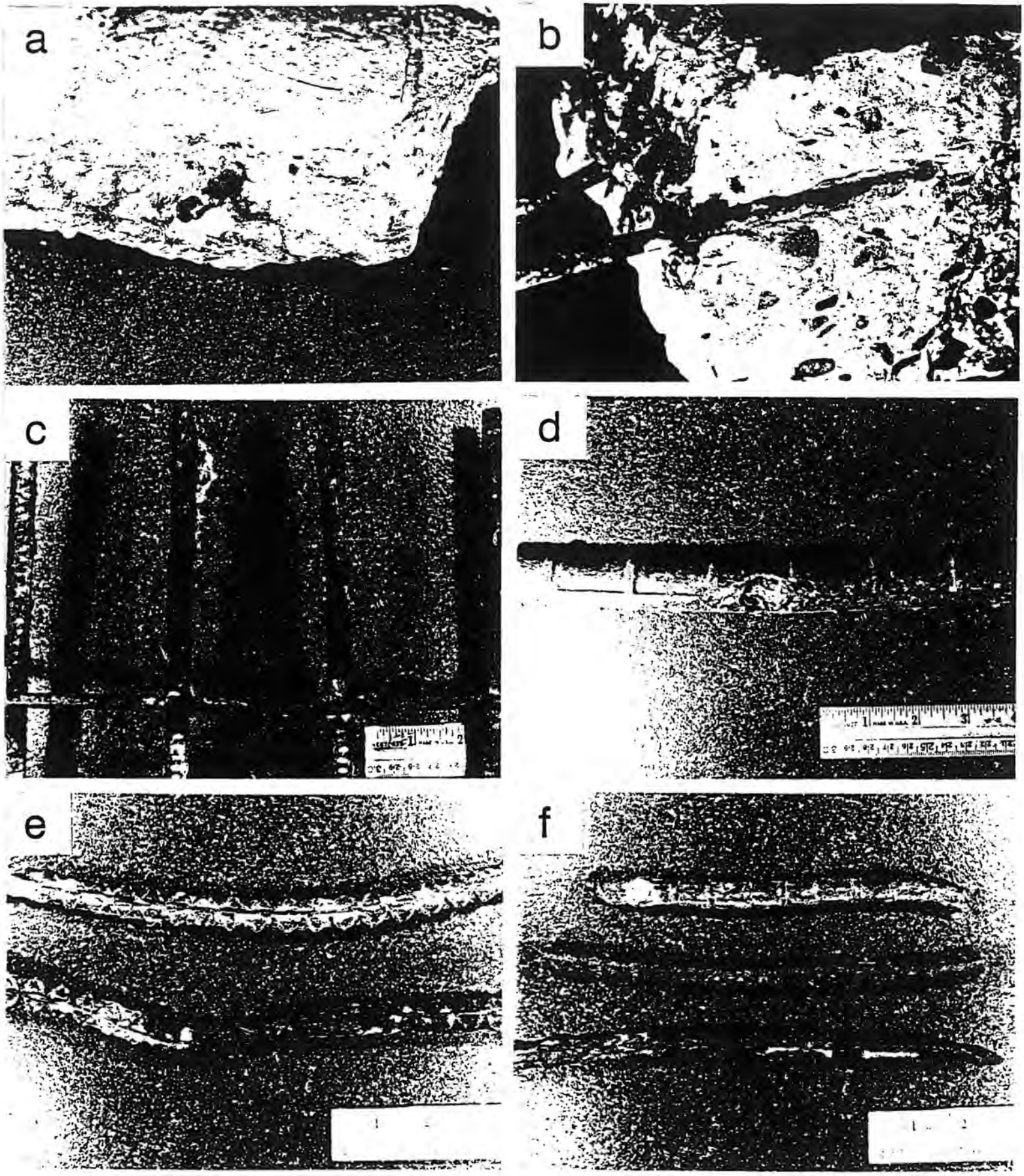


Figure 6. Corroded reinforcements with and without concrete blocks collected from the field: (a) and (b) concrete cracks around corroded reinforcements, (c) severe corrosion near grid-intersections, (d) and (e) localized corrosion near material defects (inclusions) and welded areas, and (f) reinforcement volume changes by corrosion.

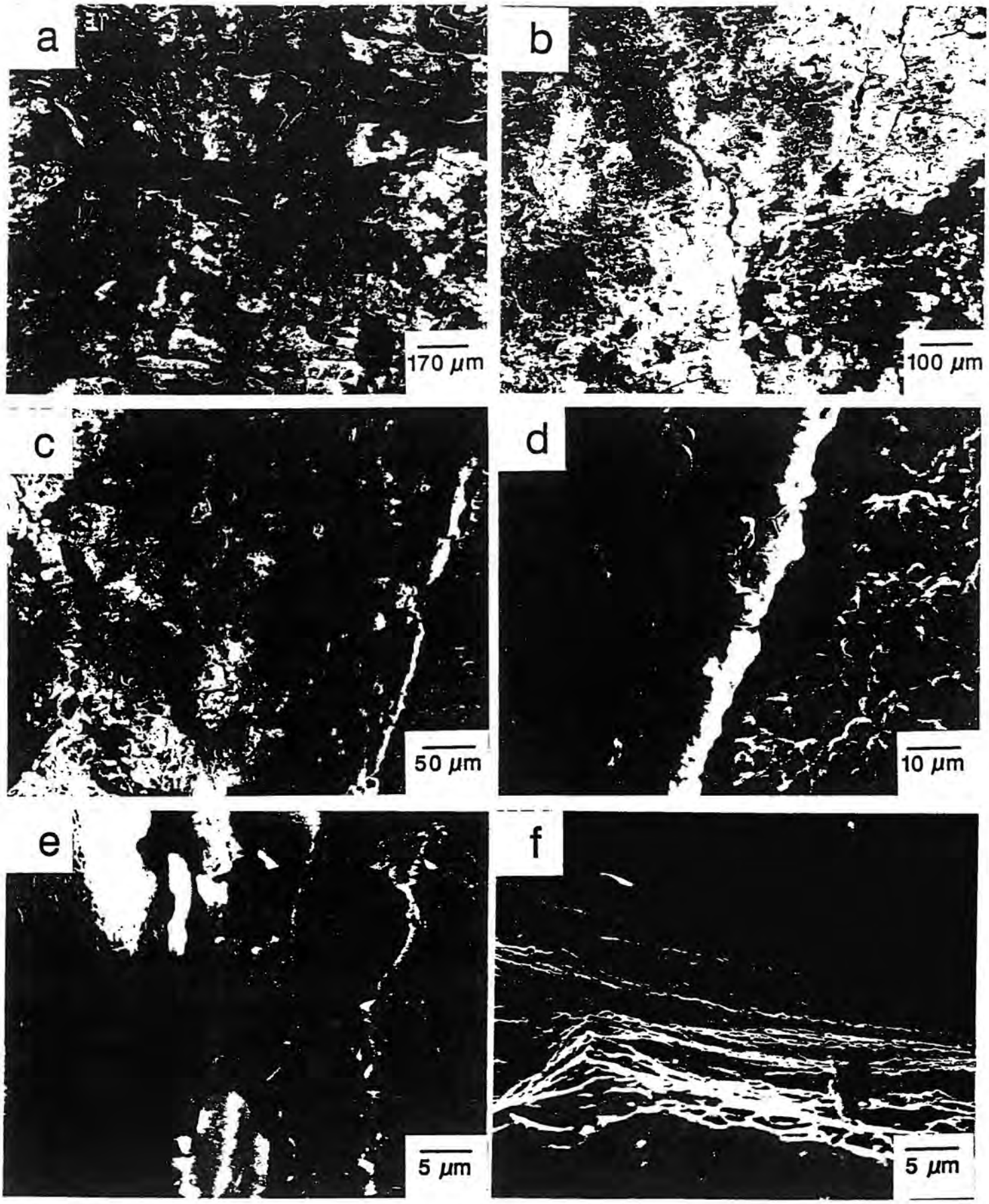


Figure 7. Surfaces of corroded reinforcement by scanning electron microscopy: (a) sharp cracks on oxide layer, (b) irregular cracks in reinforcement metal matrix, (c) and (d) corrosion initiation and propagation along grain boundaries of reinforcement material, (e) a space between oxide layer and metal matrix, and (f) crack propagation on oxide layer by fatigue stresses.

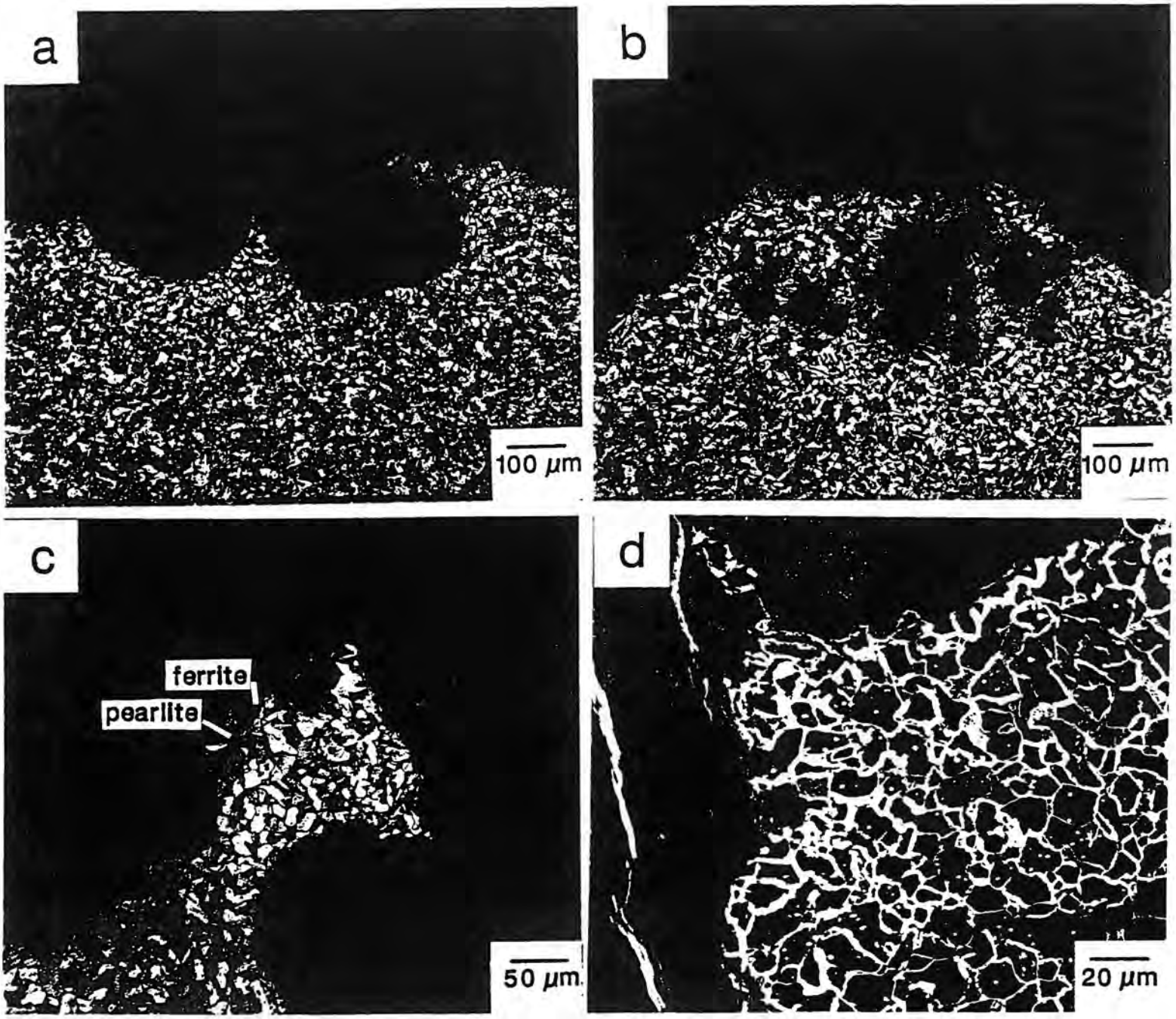


Figure 8. Cross section of corroded reinforcement by optical microscopy: (a) and (b) severe corrosion beneath the surface, (c) preferential corrosion on pearlite structure, and (d) corrosion propagation along the grain boundaries of reinforcement material.